2016

Dynamic Behavior of Composite Subjected to Maritime Environments

Sebastian Reh
University of Rhode Island, rehsebastian@my.uri.edu

DYNAMIC BEHAVIOR OF COMPOSITE MATERIALS SUBJECTED TO MARITIME ENVIRONMENTS

BY

SEBASTIAN REH

A THESIS SUBMITTED IN PARTIAL FULFILLMENT OF THE REQUIREMENTS FOR THE DEGREE OF

MASTER OF SCIENCE

IN

INDUSTRIAL AND SYSTEMS ENGINEERING

UNIVERSITY OF RHODE ISLAND

2016

MASTER OF SCIENCE THESIS

BY

SEBASTIAN REH

APPROVED:

Thesis Committee:

Major Professor: **Jyh-Hone Wang**

Arun Shukla

Richard Brown

Nasser H. Zawia

DEAN OF THE GRADUATE SCHOOL

UNIVERSITY OF RHODE ISLAND

2016

ABSTRACT

Material degradation of composite materials is a major concern in maritime applications. In this experimental investigation, effects of moisture-induced degradation, using two different salt solutions with concentrations of 1.8% and 3.7%, on reinforced epoxy composites were studied by means of designed experiments. The objective of this study is to find the change of dynamic behavior of the composite material exposed to marine environments for different time spans of weathering.

Two different layups were compared, namely the simple cross ply construction $[0°|90°]_{2s}$ and a balanced symmetric bi-axial construction $[\pm 45°]_{2s}$. The composite laminate specimens manufactured by vacuum infusion process under laboratory conditions were immersed in the two salt solutions, representing salinity levels of oceans and seas, e.g. Atlantic and Pacific Ocean, Baltic Sea and Black Sea, at accelerated weathering conditions of 65°C. The comparative study comprised three weathering stages, specimens in the non-weathered stage in a desiccated condition and specimens subject to weathering for 15 days and 30 days. Drop-weight impact tests were performed on all specimens to obtain the maximum load of this sensitive out-of-plane impact stress state.

A diffusion study was performed for all layups and solutions at two temperatures, 65°C and 25°C. Thus, the diffusion was described quantitatively to derive damage state predictions.

Diffusion curves and diffusion coefficients of both layups $[0°|90°]_{2s}$ and $[\pm 45°]_{2s}$ did not differ significantly. This is, seemingly, because both laminate constructions

possessed the same fiber volume fraction f=55%. Different salt concentrations did not penetrate the composite material with different rates.

Peak loads through drop-weight testing were significantly decreased by means of the weathering treatment. Once the composite material was saturated, no significant change of properties occurred for the 30 days period at the accelerated diffusion rate.

Comparing both layups, the angle ply laminate significantly bore a higher amount of out-of-plane load in both, the non-weathered and weathered specimens in the lower salt concentration. Exceeding certain salinity, in this study reached through the higher salt concentration of 3.7%, the peak loads through impact testing became alike for both layups.

ACKNOWLEDGEMENTS

I would first like to acknowledge and thank my advisor, Dr. Jyh-Hone Wang, for all of his guidance and support through this project. His guidance and mentoring has helped me significantly to grow as a scientist and individual.

Furthermore, I would like to thank my co-advisor, Dr. Arun Shukla for introducing me into his Dynamic Photo Mechanics Laboratory and his persistent support during my studies at the University of Rhode Island. I would also like to thank the other professors who have helped me along my academic career, particularly Prof. Dr.-Ing. Karin Schäfer for her guidance, enthusiasm and all that I have gained from her teaching. I would like to thank Dr. Richard Brown and Dr. Christopher Baxter for agreeing to serve as my committee members.

Much of my success would not have been possible without the help of my colleagues in the Dynamic Photo Mechanics Laboratory: Helio Matos, Carlos Javier, Chris Shillings, Michael Pinto, Craig Tilton, Emad Makki, Erin Gauch, Prathmesh Parrikar, Nicholas Denardo and Shyamal Kishore. I would also like to thank Dave Ferreira, Joe Gomez, Jim Byrnes, Jen Cerullo and the rest of the mechanical and industrial and systems engineering department faculty and staff.

The Support of NSWC under grant no. N00174-16-C-0012 for use of materials and facilities is greatly appreciated. Thanks to TPI Composites for their help in fabricating the composite materials.

Last and certainly not least, I would like to thank my family and friends for their constant love and support through all small and big challenges.

Table of Contents

List of Figures

List of Tables

1 INTRODUCTION

Composite materials in marine applications are gaining popularity. Carbon fiber as reinforcement in polymer matrices can be found in an increasing number of applications. Composites have been used in fields such as aircrafts, automotive and transportation industry, boat and shipbuilding, as well as sports equipment. The renewable energy sector is a rising field in engineering. Components for wind turbines and tidal turbines have prompted an interest in composite materials' behavior in maritime environments.

The degradation of composite materials in maritime environments depends on a variety of factors. While adverse effects on material properties are generally expected through moisture diffusing into polymeric composite materials [1, 2], enhancement of mechanical properties through moderate water uptake in reinforced polymer composites has been observed [3]. Polymeric composites' responses can be very complex, especially in dynamic situations. Factors include polymer resin properties, arrangement and architecture of fibers and thickness of laminate [4–7].

Understanding the dynamic response of composites before and after material degradation through weathering, can help to predict the long-term suitability of light weight structures using reinforced polymer composites.

The impact response on composite laminate has been studied in the past [2, 4–8]. However, none of these studies discuss the influence of saline solution on composite material properties. Several studies focused on the fatigue strengths of laminates in marine use [9] and sandwich constructions under extreme environments [10].

The present study focuses on the change of low-velocity impact response through moisture-induced degradation on reinforced epoxy composites. High salinity differences occur depending on the ocean and the exact location within that water. Salt solutions of 1.8% and 3.7% represent the average concentrations in several bodies of water such as the Atlantic and Pacific Ocean, Baltic Sea, and Black Sea. Two commonly used laminate architectures were compared, the simple cross ply construction $[0°|90°]_{2s}$ and a balanced symmetric bi-axial construction $[\pm 45°]_{2s}$. The assessment method is primarily comparative by employing the statistical tool Analysis of Variance. Prolonged seawater exposure within a shorter period of experimental time of 15 days and 30 days is realized by artificially furthering the degradation process through submersion at elevated temperature of 65°C.

2 LITERATURE REVIEW

2.1 Degradation of Polymers and Polymeric Composites

2.1.1 Overview of Material Degradation Agents

Since degradation of materials can be triggered by a number of different agents, the phenomenon is commonly subdivided into: (i) Moisture-Induced Degradation, (ii) Thermo-Oxidative Degradation, (iii) Photodegradation and (iv) Stress-Induced Degradation. Note that two degradation agents may have a synergetic effect in combination, so that the sum is greater or lesser than their individual effects. Moreover, the degradation caused by cyclic exposure may differ from the equivalent amount of continuous exposure. The aforementioned degradation types are valid for but not limited to polymers and their derivative materials.

2.1.2 Moisture Diffusion in Polymers and Polymeric Composite Materials

It is widely recognized that moisture plays a significant role in influencing the mechanical properties of polymers and polymeric composite materials. Observing polymeric composite materials, the polymer matrices are hygroscopic and thus responsible for water sorption while the water uptake of glass fibers or carbon fibers is negligible [3]. A significant reduction in the modulus, strength, and glass transition temperature (T_g) can be caused by exposure to moisture [9–13]. Characteristics of moisture absorption and desorption polymer or polymeric composites can provide qualitative as well as quantitative insight into the degradation mechanism present in the material.

Diffusion in Polymers

The amount of water penetrating into polymers varies widely. At low degrees of absorption, only a small degree of reversible swelling is produced. In the simplest case of unidirectional diffusion without edge effects, the mass uptake at saturation is independent of the sample thickness h. The diffusion into the polymer then obeys Fick's second law[14]:

$$\frac{\partial C}{\partial t} = D\frac{\partial^2 C}{\partial z^2} \tag{1}$$

where C is the local water concentration, D the diffusion coefficient and z the depth of the layer in the sample thickness. The resolution of this differential equation gives [15]:

$$\frac{C_t}{C_s} = 1 - \frac{4}{\pi}\sum_{n=1}^{\infty}\frac{1}{2n-1}\cos\left((2n-1)\pi\frac{z}{h}\right)e^{\left(-(2n-1)\pi^2\frac{Dt}{h^2}\right)} \tag{2}$$

where C_s is the concentration at saturation, C_t the concentration at time t, h the sample thickness. The whole mass uptake m_t at time t is given by [14]:

$$\frac{m_t}{m_s} = 1 - \frac{8}{\pi^2}\sum_{n=1}^{\infty}\frac{1}{(2n-1)^2}e^{\left(-(2n-1)\pi^2\frac{Dt}{h^2}\right)} \tag{3}$$

where m_s is the mass uptake at saturation.

Equation (3) can be well approximated by the following equation [14, 16]:

$$\frac{m_t}{m_s} = \frac{4}{h}\sqrt{\frac{Dt}{\pi}} \tag{4}$$

where m_t is water mass absorbed at the time t, m_s is saturated water mass, D is the diffusion coefficient and h is the plate thickness. Equation (4) can be simplified for an

arbitrary ratio of $\frac{m_t}{m_s}$ which is low enough before saturation mass uptake is reached, e.g. $\frac{m_t}{m_s} = 0.5$. A solution of D can then be approximated with:

$$D = 0.049 \frac{h^2}{t_{50}} \tag{5}$$

where t_{50} defines the time after 50% mass gain is obtained. In the simplest case, water diffusivity depends on temperature according to an Arrhenius law:

$$D = D_c \, e^{-\frac{E_a}{RT}} \tag{6}$$

where D is the diffusion coefficient at absolute temperature T, D_c is a constant, E_a is Activation Energy, and R is the universal gas constant.

At larger degrees of absorption, polymers may follow a path different to Fick's law. Irreversible water sorption underlies cracking arising from swelling stresses [17] or the existence of inhomogeneities on the nanoscale [18, 19]. Water molecules in polymeric materials can be distinguished between two states [20]. Unbound or free state of water is attributed to water molecules that exist in inhomogeneities of the material such as voids and nanopores [21]. On the other hand, bounded water molecules interact with polymer chains through hydrogen bonding or other chemical reactions.

A schematic of damage mechanisms of a polymeric composite material from water absorption is displayed in Fig. 1. Additionally to the mentioned damage mechanism, capillary action through cracks in the matrix and at the interface of matrix and fiber (wicking), leaching of the matrix, crack initiation at interfacial voids and residual stresses at the interface can be observed.

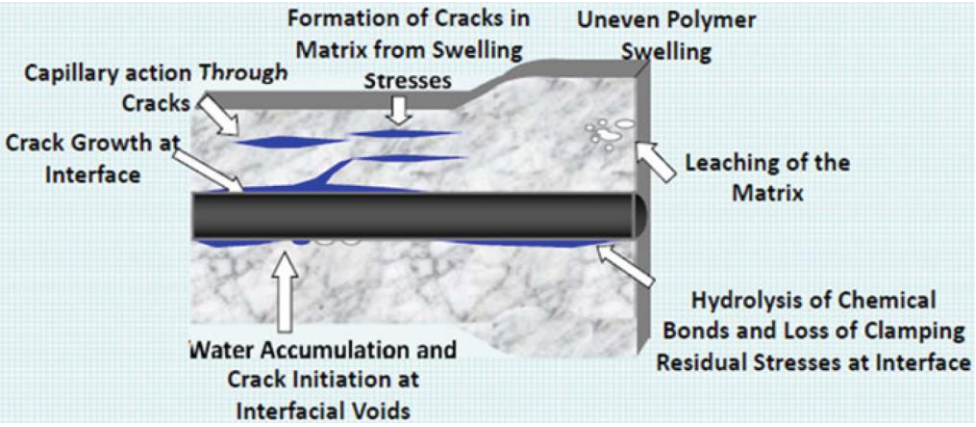

Fig. 1: Damage Mechanisms of a Polymeric Composite Material from Water Absorption [14]

Non-Fickian or anomalous diffusion as shown in Fig. 2 is likely to occur when a polymer composite laminate is subjected to external stresses that could give rise to internal damage in the form of matrix cracks. As a result, it is necessary to take the combined effects of temperature, stress (or strain), and damage in the construction of such a model into account [11].

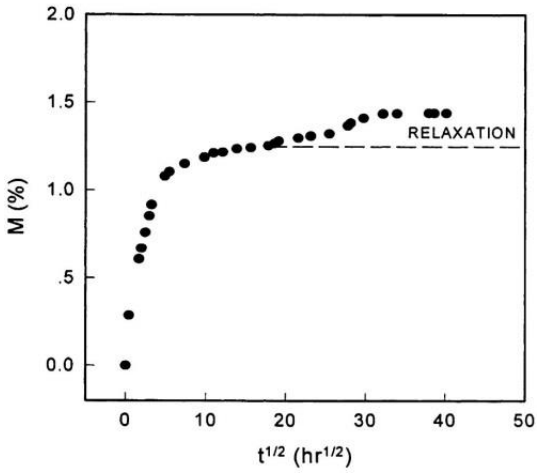

Fig. 2: Water Uptake for Diffusion Exhibiting Two Equilibrium Stages Seemingly Due to Polymer Swelling and Physical Relaxation Measured at 70°C [1]

Diffusion in Composite Materials

The homogeneity of the polymer, thus the diffusion in polymeric composite materials is disrupted by reinforcing fibers. Water diffusivity in a unidirectional laminate with a fiber volume fraction f is reduced by the fiber volume. The water flux in the longitudinal direction is thus expected to be proportional to the matrix cross section following [14]:

$$D_{||} = D_m(1 - f) \tag{7}$$

where $D_{||}$ is the overall diffusivity along fiber direction, D_m the diffusion coefficient of pure resin and f the fiber volume fraction. In the transverse direction, impermeable fibers impose a certain tortuosity to diffusion pathways. There are many expressions for the corresponding overall diffusivity in transverse direction D_t, the simplest one being derived from the Maxwell–Garnett approximation [14]:

$$\frac{D_t}{D_m} = \frac{1 - f}{1 + f} \tag{8}$$

Note, that the frequently used one-dimensional Fickian model tends to overestimate the moisture absorption in panels for short diffusion times, even when it is modified to take into account edge effects [11].

2.2 Experimental Data Analysis – Analysis of Variance

Highly sensible responses and small changes in magnitude require an appropriate tool to analyze the experimental data. An effective, flexible and universally applicable method of data analysis for experimental sciences is given by the Analysis of Variance (ANOVA). The idea and advantageous applicability of ANOVA to various fields of research has been shown frequently [22, 23]. In the following, the ANOVA method is illustrated using a single factor experiment. Consider an experiment involving two groups of subjects, e.g. a specific material in its original state (μ_0) and the same material treated in some way (μ_1) e.g. exposed to sea water with a salinity of 3.7%. At the end of the experiment, a measurement (y) is taken from each subject. To test the null hypothesis that there is no difference between the two means e.g., $\mu_0 - \mu_1 = 0$, a statistical test method like the Student 's t-test could be employed [22]. The statistic t evaluates the ratio of difference between the two means and measures the variation between the individual subjects pooled from both groups of subjects.

In one exemplary case it becomes apparent how the Analysis of Variance (ANOVA) may be advantageously employed in such case [22]. If the t-test method of analysis is employed for more than two different groups of subjects, e.g. because more concentration levels of salinities are being used (e.g. μ_0, μ_1 and μ_2), there would be the same amount of t-tests necessary as amounts of different groups are existent. However, logical dependent conclusions could be made without testing all combinations (μ_0 vs. μ_1, μ_0 vs. μ_2 and μ_1 vs. μ_2), e.g. if $\mu_0 > \mu_1$ and $\mu_0 = \mu_2$ then it must be true that $\mu_2 > \mu_1$. Hence, the conclusion follows from the previous two tests and is not being drawn independently.

ANOVA delivers a single statistical test to find about whether the means of the groups of subjects (treatment) differ significantly. It allows considering replications within the same treatment and is therefore advantageous in terms of data analysis. The results of the experiment y_{ij}, also called observations, the sums of each treatment i: $y_{0.}, y_{1.}, y_{2.}$ and the treatment means $\overline{y_0}$, $\overline{y_1}$ and $\overline{y_2}$ are implied through Table 1.

The name analysis of variance is derived from a partitioning of total variability into its components. The measure of overall variability in the data can be expressed as:

$$Total\ sums\ of\ squares\ SS_T = \sum_i \sum_j (y_{ij} - Y^*)^2 \qquad (9)$$

where Y^* is the overall mean and y_{ij} is representing an observation in a one factor experiment with n replications. The sums of squares can serve as a measure of influence of the treatment effects when calculated for each treatment independently. If there is no significant difference between the treatment means, there will be no significant variation of these means from their overall mean Y^*. The measure of treatment variation is defined as:

$$Between\ treatments\ sums\ of\ squares\ SS_{BT} = n \sum_j (y_{i.} - Y^*)^2 \qquad (10)$$

where Y^* is the overall mean, $y_{i.}$ the treatment total for treatment i and n replications.

Table 1: Typical Data for a Single-Factor Experiment with three levels (treatments)

	Treatments		
Replication	Treatment 0	Treatment 1	Treatment 2
1	y_{01}	y_{11}	y_{21}
2	y_{02}	y_{12}	y_{22}
3	y_{03}	y_{13}	y_{23}
Totals	$y_{0.}$	$y_{1.}$	$y_{2.}$
Averages (Means)	$\overline{y_0}$	$\overline{y_1}$	$\overline{y_2}$

In addition, there is variation between the replicate subjects within each treatment. This variation is herein referred as residual and describes the natural or random variation between experimental subjects. The total sums of squares can be calculated by:

$$\begin{aligned} &Total\ sums\ of\ squares\ SS_T \\ &\quad = Between\ treatments\ sums\ of\ squares\ \ SS_{BT} \\ &\quad + Error\ sums\ of\ squares\ SS_E \end{aligned} \tag{11}$$

To compare the between treatments and error mean squares, the sums of squares are divided by the appropriate degrees of freedom (DF), respectively, according to the ANOVA Table 2. These measures are called variance or mean square of the between treatments sum of squares and error sum of squares. Testing the variance ratio of these sources of variation is the basis of an ANOVA. Comparing the F-value, which indicates the number of times the between treatment mean square exceeds that of the error mean square, to the F-probability distribution, delivers certainty if the null hypothesis (equal treatment means) is rejected. The level of certainty is previously defined by the significance level α.

Table 2: Analysis of Variance Table for the Single-Factor, Fixed Effects Model

Source of variation	DF	Sum of Squares	Mean square	F
Between Treatments	a-1	SS_{BT}	$MS_{BT} = \frac{SS_{BT}}{\mathrm{a}-1}$	$F_0 = \frac{MS_{BT}}{MS_E}$
Error (within treatments)	N-a	SS_E	$MS_E = \frac{SS_E}{\mathrm{N}-\mathrm{a}}$	
Total	N-1	SS_T		

Where a is the number of different treatments (levels), N is the total number of observations, MS_{BT} is mean square between treatments, MS_E mean square of error and F the variance ratio, DF is the number of degrees of freedom.

The ANOVA presumes that (i) observations are independent, (ii) observations have a constant variance σ^2 and (iii) observations are normally distributed.

Generally, the common procedure in hypothesis testing after determining a statistical model is to specify a value for a significance level α. As mentioned before, it is then possible to state whether a potential null hypothesis is or is not rejected at the specified α-value, also called level of significance. A typical level of significance is chosen with α = 0.05 [23]. This significance level approach using the F-value may be unsatisfactory because it does not provide the decision maker enough information regarding the location of the computed value within the rejected region. For this reason, the widely adopted p-value approach can be utilized in addition to the first approach. The p-value is the probability that the test statistic will adopt a value that is at least as extreme as the observed value of the statistic when the null hypothesis is true. In other words, the p-value is the smallest level of significance that would lead to rejection of the null hypothesis H_0 [23].

Having the background in degradation of composite materials and the theory of experimental data analysis, the next sections cover information about the composite material and its architectures used.

3 MATERIALS

3.1 Composite Material

The tested materials in this study are symmetric and balanced carbon fiber/epoxy composite laminates. Two different laminate layups are studied, a cross-ply construction $[0°|90°]_{2s}$ and a symmetric bi-axial construction $[\pm 45°]_{2s}$ (Fig. 4). The composite plates are self-manufactured in the facilities and with the help of TPI Composites Inc. (Warren, RI) and at the University of Rhode Island's laboratories. The biaxial carbon fiber fabric Carbon XC611 from Gurit reinforces the epoxy resin system RIMR 135/RIMH 137 from Momentive. This biaxial carbon fiber fabric is arranged in a double-layer stitched [±45°] layup possessing an areal weight of 602g/m².

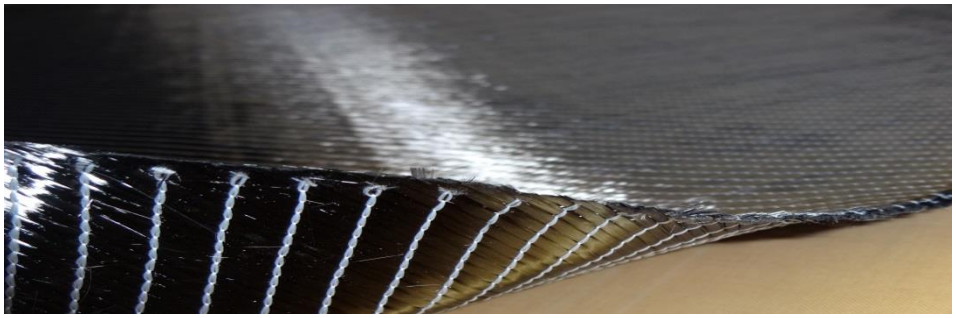

Fig. 3: Biaxial Carbon Fiber Fabric Arranged in a Double-Layer Stitched [±45°]-Layup

The finished carbon fiber/epoxy plates consist of four orthogonal unidirectional layers with a total nominal thickness of 1.28mm. The composite material's density is 1.501g/cm³ determined according to ASTM D792 Density and Specific Gravity (Relative Density) of Plastics by Displacement [24] in deionized water. A fiber volume fraction of the material of $f = 55 \pm 2\%$ is reached. A glass transition temperature of 86°C is determined using dynamic scanning calorimetry (DSC) after curing the

composite plate. An image of the laminate constructions of the composite material can be seen in Fig. 4.

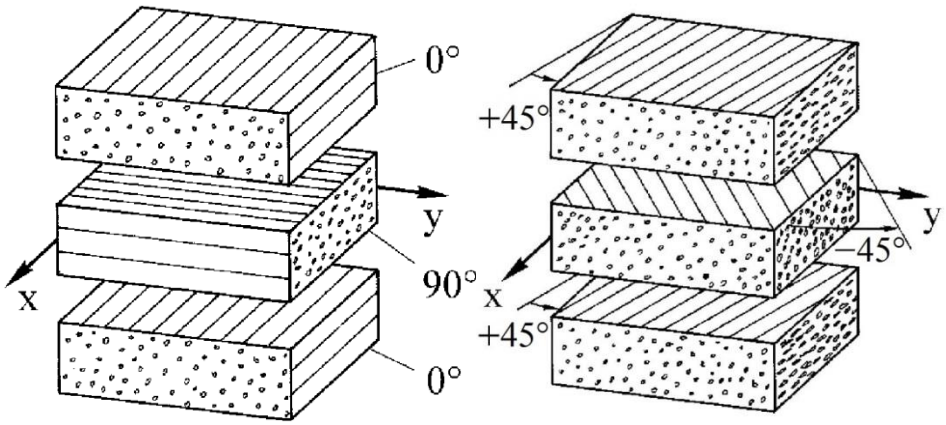

Fig. 4: Cross Ply Layup L1 and Angle Ply Layup L2 [3]

3.2 Manufacturing of Composite Plates

The composite plates, both the double cross-ply layup and the $[\pm 45°]_{2s}$ layup, are manufactured in a single-bag vacuum infusion process (Fig. 5). Panels with the size of 0.69m x 0.69m, allow homogeneous infusion of the low viscosity epoxy. The same type of fabric is used for both layups. Changing the orientation of cutting the fabric (1) along/normal to the fibers and (2) turned by 45°, results in the desired fiber orientation, respectively. The mixing ratio of the resin and hardener is chosen according to the technical data sheet of the epoxy system to be 100:30 parts per weight. The two-component epoxy resin system is pre-cured at 40°C for 24hrs and post-cured at 70°C for 10hrs. A characteristic and repeatable surface is achieved by applying peel ply illustrated in Fig. 6. With the applied vacuum pump a pressure difference below the atmospheric pressure of up to 800mbar can be reached, called gauge vacuum.

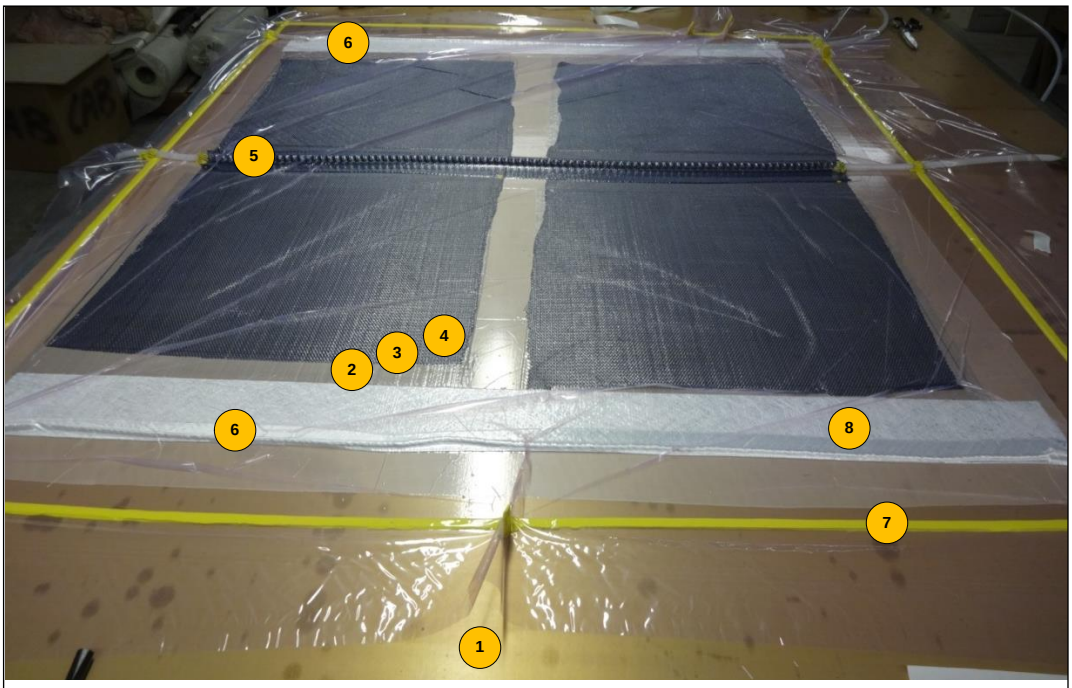

1. work space - Teflon surface
2. carbon fabric
3. peel ply
4. distribution mesh
5. feeding line
6. vacuum pump line
7. sealing tape
8. cavities
9. vacuum foil

not depicted:

10. catch pot
11. vacuum pump

Fig. 5: Set-up of Vacuum Infusion of Carbon Fiber Reinforced Epoxy

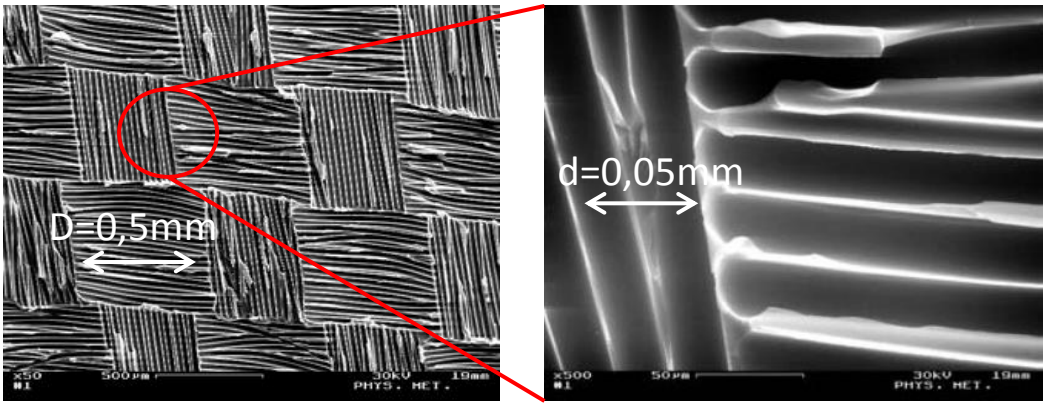

Fig. 6: Dimensions and Pattern of Peel Ply Magnified by Microscope [3]

3.3 Specimen Preparation

The manufactured composite panels are cut into specific dimensions. Specimens are prepared to serve in a dynamic impact experiment. A table saw with a diamond blade is utilized to achieve a precise cut and avoid delamination and fiber breakage near the edges of the material. This procedure also supports an even exposure within the weathering setup. Table 3 displays the specimen dimensions for the low-velocity impact test. Dimensions are chosen to meet experimental specifications including ASTM standard D7136/D7136M (drop-weight impact event) and obtain feasibility of planned experimentation.

Table 3: Dimensions of Drop-Weight Specimens

Drop-weight specimens	Length l	Width w	Thickness h
Dimensions in mm	152.4	101.6	1.28

All specimens are cleaned and freed from superficial impurities with Methanol after cutting. Prior to the actual experimentation, all specimens are desiccated in indicating silica gel to extract atmospheric moisture. The indicating silica gel changes color when it has absorbed 6% of its weight in moisture showing the point of replacement.

Table 4: Exemplary Mechanical Data of Carbon Fiber Reinforced Epoxy Resin System* [25]

Static Test Property	Carbon Fiber Reinforced Epoxy
Flexural Strength (N/mm²)	720 – 770
Tensile Strength (N/mm²)	510 – 550
Compressive strength (N/mm²)	460 – 510
Interlaminar shear strength (N/mm²)	47 – 55
Modulus of elasticity (kN/mm²)	40 – 45

*8 layers of carbon fabric, plain, 200g/m² (5.0oz/sq.yd.) 2mm (0.08in) thick

4 DESIGN OF EXPERIMENT

The aspect of out-of-plane impact loading of previously degraded composite material laminates shall be the subject of the present study. It hereby seeks to understand the change of mechanical behavior of composite materials subjected to an impact event after exposure to marine conditions by means of accelerated lifetime testing. A typical material property experiment for this purpose is a drop-weight impact test at low velocities.

4.1 Response, Factors and Levels Considered

Mainly, the maximum load after such experiments can be analyzed to determine the out-of-plane strength. Additionally, the absorbed energy of the specimens is a relevant response that gives insight into the dynamical behavior by representing the material's toughness. The peak load is being analyzed as the main response from the statistical experiment.

The study focuses on different factors of influence during the weathering of the composite material. Firstly, the weathering time is expected to have an influence on the dynamic behavior of the tested material. It is defined as the time of exposure of the composite material to the salt solution. Secondly, the salinity is expected to significantly affect the absorption rate and thus degradation of the tested material. Generally, the salinity describes the relative concentration of salt in a watery medium. More specifically, the exact definition according to the ASTM standard is evaluated on in the experimental set-up (5 Experimental Procedure). Thirdly, the structure of the composite material can be considered a blocking factor, herein referred as layup.

Each factor consists of different levels with inherent properties. The factor weathering time has been defined to possess three levels including the non-weathered stage, 15 days and 30 days of exposure to the salty medium. The amount of levels has been chosen in such way to gather data points at a non-weathered stage, a partially saturated and a fully saturated composite material. Hence, a comparative evaluation of those characteristic points produces a thorough description of development of the degraded material.

The factor salinity is subdivided into two levels. These concentration levels follow the average salt content of Pacific and Atlantic Ocean and other international waters such as the Baltic Sea and the Black Sea. Thus, the gained results can be used for applications in the corresponding area. Table 5 shows an overview of the various salinities in the oceans as the mass percentage. The solution 1 carries 1.8% of salt whereas solution 2 contains 3.7% of salt.

Table 5: Salinities in Oceans, Mass Percentage [26]

Oceans	Salinity (Mass. %)
Atlantic Ocean	3.0 – 3.7
Bering Sea	3.4 – 3.5
Irish Sea	3.4 – 3.7
Indic Ocean	3.4
Caspian Sea	1.0 – 3.0
Mediterranean Sea	3.6 – 3.9
Arctic Ocean	3.0 – 3.5
Northern Sea	3.5
Baltic Sea	0.3 – 1.8
Pacific Ocean	3.45
Persian Gulf	4
Red Sea	3.7 – 4.3
Black Sea	1.7 – 1.8
Dead Sea	29

In order to build up a broader database to describe the dynamic behavior of the composite material, two different layups will be subject of the study. A cross-ply laminate $[0°|90°]_{2s}$ (L1) and a bi-axial laminate $[\pm 45°]_{2s}$ (L2) compose the only two-level blocking factor in the design of experiment.

Table 6: Statistical Input Variables and Responses

Variable	Description	Levels
Response	Maximum Load (kN)	Continuous response
Factor 1	Weathering time (days)	0 days, 15 days, 30 days
Factor 2	Salinity (%)	1.8%, 3.7%
(Blocking) Factor 3	Layup (L)	L1=$[0°\|90°]_{2s}$, L2=$[\pm 45°]_{2s}$

4.2 Statistical Model and Hypotheses

A statistical model describes the response's mean value taking all main factors, interactions of factors, blocking factors and the random error of an experiment into account. A statistical model allows for hypothesis testing. A statistical hypothesis is a statement with reference to either the parameters of a probability distribution or the parameters of a model.

The subsequent equation shows the statistical model specifically designed for this study following a two-factor blocked factorial design.

$$y_{ijkl} = \mu + \tau_i + \beta_j + (\tau\beta)_{ij} + \delta_k + \epsilon_{ijkl} \tag{12}$$

with $i = \{1,2,3\}; j = \{1,2\}; k = \{1,2\};\ l = \{1,2,3,\dots,7\}$

Therein, the observations y_{ijkl} are described by the overall mean of the main response peak load μ, the first main factor weathering time τ_i, the second main factor salinity β_j, their interaction weathering time with salinity $(\tau\beta)_{ij}$, the blocking factor layup δ_k and the random error ϵ_{ijkl}. Each observation y_{ijkl} is assigned one level of the introduced factors where the weathering times are part of $i = \{1,2,3\}$, the salinities $j = \{1,2\}$ and the layups $k = \{1,2\}$. The replications per factor combination are considered by $l = \{1,2,3,\dots,n\}$ where the sample size equals $n = 7$. Evaluation of preliminary test data serves to estimate the necessary sample size which will be shown later. The model assumes that (i) observations are independent, (ii) observations have a constant variance σ^2 and (iii) observations are normally distributed.

Generally, the common procedure in hypothesis testing after determining the statistical model is to specify a value for a significance level α. It is then possible to state whether a potential null hypothesis is or is not rejected at the specified α-value or level of significance. A typical level of significance is chosen with $\alpha = 0.05$ [23]. This significance level approach may be unsatisfactory because it does not provide the decision maker enough information regarding the location of the computed value within the rejected region. For this reason, the widely adopted p-value approach will be utilized in addition to the first approach. The p-value is the probability that the test statistic will adopt a value that is at least as extreme as the observed value of the statistic when the null hypothesis H_0 is true. In other words, the p-value is the smallest level of significance that would lead to rejection of the null hypothesis H_0 [23].

Regarding the formulation of the hypotheses, the results of a series of experiments are used to state whether the factors weathering time, salinity and their interaction with their inherent levels, respectively, are significant factors to change the response. Table 7 shows an overview of the analyzed hypotheses of the statistical experiment.

Table 7: Hypotheses of Statistical Experiment

Factor	Hypotheses
Weathering time	Hypothesis H_0: weathering time is not significant Hypothesis H_1: weathering time is significant
Salinity	Hypothesis H_0: salinity is not significant Hypothesis H_1: salinity is significant
Interaction: Weathering time*salinity	Hypothesis H_0: Weathering time*salinity is not significant Hypothesis H_1: Weathering time*salinity is significant

The blocking factor layup is expected to be significant and is therefore not further mentioned for hypothesis testing.

4.3 Experiment Designs

All of the aforementioned factors are combined in an experimental design. The Randomized Complete Block Design uses the design techniques of randomization and blocking to decrease variability arising from a nuisance factor (Table 8 and Table 9 and [23]). In the full model the Two-Factor Blocked Factorial Design is applied (Table 10) allowing analysis of a potential interaction between factors.

The first experiment design (Design 1) focuses on the influence of the weathering time for each salinity separately. It seeks to understand the degradation occurring in the material over the time. Both layups L1 and L2 are tested for each salinity and weathering time.

The second experiment design (Design 2) compares the different stages of weathering while both salinity levels can be linked to each other. Since a differentiation between the two salinity levels would deliver the exact same values and would warp the statistical analysis, the non-weathered stage at weathering time, is not taken into consideration. The comparison of the weathering times, 15 days and 30 days, and the salinity levels, 1.8% and 3.7%, as well as their interaction provides the necessary information in order to judge the formulated hypotheses.

Table 8: Experiment Design 1 as Randomized Complete Block for Low Salinity 1.8%

Low Salinity			
	Weathering Time		
Layup	0 days	15 days	30 days
L1	$y_{1111}, y_{1112}, \cdots y_{1117}$	$y_{2111}, y_{2112}, \cdots y_{2117}$	$y_{3111}, y_{3112}, \cdots y_{3117}$
L2	$y_{1121}, y_{1122} \cdots y_{1127}$	$y_{2121} y_{2122}, \cdots y_{2127}$	$y_{3121}, y_{3122} \cdots y_{3127}$

Table 9: Experiment Design 1 as Randomized Complete Block for High Salinity 3.7%

High Salinity			
	Weathering Time		
Layup	0 days	15 days	30 days
L1	$y_{1211}, y_{1212} \cdots y_{1217}$	$y_{2211}, y_{2212} \cdots y_{2217}$	$y_{3211}, y_{3212} \cdots y_{3217}$
L2	$y_{1221}, y_{1222} \cdots y_{1227}$	$y_{2221}, y_{2222} \cdots y_{2227}$	$y_{3221}, y_{3222} \cdots y_{3227}$

Table 10: Experiment Design 2 as Blocked Factorial Design

		Weathering Time	
Salinity	Layup	15 days	30 days
Low Salinity	L1	$y_{2111}, y_{2112}, \cdots y_{2117}$	$y_{3111}, y_{3112}, \cdots y_{3117}$
	L2	$y_{2121} y_{2122}, \cdots y_{2127}$	$y_{3121}, y_{3122} \cdots y_{3127}$
High Salinity	L1	$y_{2211}, y_{2212} \cdots y_{2217}$	$y_{3211}, y_{3212} \cdots y_{3217}$
	L2	$y_{2221}, y_{2222} \cdots y_{2227}$	$y_{3221}, y_{3222} \cdots y_{3227}$

4.4 Sample Size and Randomization

Evaluation of preliminary test data serves to estimate the necessary sample size. The data points are taken from a similar composite material Carbon/Epoxy plate with a woven fabric structure. The material was subject to weathering for 30 days in a 3.5% sodium chloride solution in a former student research project at the University of Rhode Island. Table 11 shows the values for the maximum Load and the difference between the non-weathered and the 30 days weathered value, respectively.

Table 11: Preliminary Data: Maximum Load

	Load in kN		
No.	Non-Weathered	Weathered	Delta
Exp1	5.147	4.810	0.336
Exp2	4.980	4.871	0.109
Exp3	5.187	4.613	0.573
Exp4	4.974	4.865	0.108
Exp5	5.355	4.942	0.412
Mean	5.128	4.820	0.308
St. Dev	0.1419	0.112	0.1798

where St. Dev. is Standard Deviation

Assuming a power of 90%, a significance level of 5% and a maximum difference of the peak load of 0.336kN, a sample size power curve analysis was performed with the statistics software Minitab. A minimum amount of seven specimens for each combination of weathering time, salinity level and layup was determined (Fig. 7), leading to the sample size of seven specimens for this study.

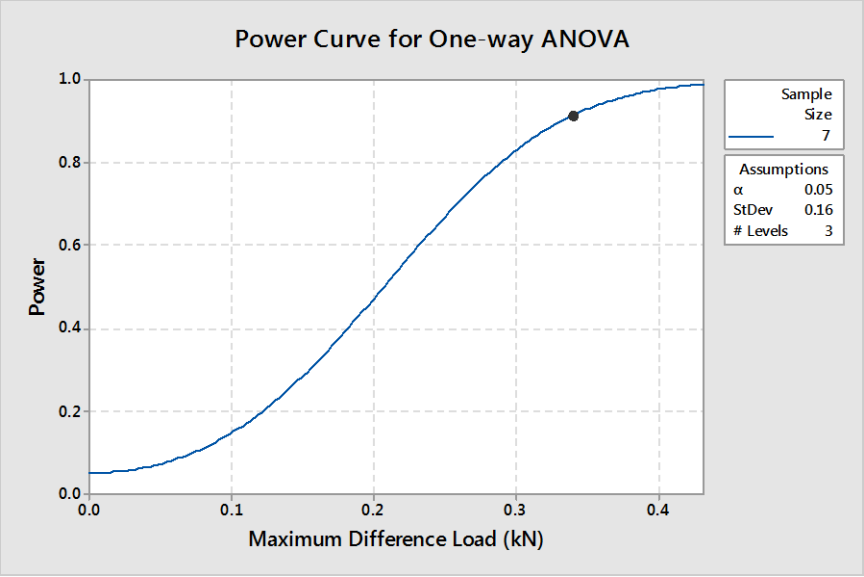

Fig. 7: Determination of Minimum Sample Size Based on Preliminary Tests

Randomization

According to the chosen designs, all experimental tests and replications should be conducted in a random order. The specimens will be placed into the weathering facilities simultaneously while the testing will be performed after the according weathering time. There is a limitation to the randomization due to this approach. Only those weathering series that are tested on the same day can be ordered randomly. Results are not expected to be influenced because ambient conditions are kept steady for all experimental trials. Each specimen is assigned a specimen ID before the actual weathering starts. The randomized experiment order for each weathering series on the different testing days is shown in Table 12 -

Table 14.

Table 12: Random Experiment Order: Solution 1/2, Layup L2, Weathering Time 15 days

Randomized experiment order	Weathering series	ID of specimen
1	sol1_L2_15d	2
2	sol2_L2_15d	2
3	sol2_L2_15d	7
4	sol2_L2_15d	6
5	sol1_L2_15d	5
6	sol2_L2_15d	5
7	sol1_L2_15d	3
8	sol1_L2_15d	4
9	sol1_L2_15d	6
10	sol2_L2_15d	1
11	sol1_L2_15d	7
12	sol1_L2_15d	1
13	sol2_L2_15d	4
14	sol2_L2_15d	3

Table 13: Random Experiment Order: Solution 1/2, Layup L1/L2, Weathering Time 30 days

Randomized experiment order	Weathering series	ID of specimen
1	sol1_L1_30d	5
2	sol1_L2_30d	5
3	sol2_L2_30d	2
4	sol1_L2_30d	7
5	sol1_L1_30d	4
6	sol2_L1_30d	4
7	sol1_L1_30d	7
8	sol1_L1_30d	2
9	sol1_L2_30d	1
10	sol2_L2_30d	1
11	sol2_L2_30d	3
12	sol2_L1_30d	3
13	sol2_L1_30d	6
14	sol2_L1_30d	5
15	sol1_L2_30d	4
16	sol1_L2_30d	2
17	sol2_L2_30d	4
18	sol1_L2_30d	6
19	sol2_L1_30d	7
20	sol2_L1_30d	1
21	sol2_L2_30d	5
22	sol1_L1_30d	3
23	sol2_L2_30d	6
24	sol1_L1_30d	6
25	sol1_L1_30d	1
26	sol2_L1_30d	2
27	sol1_L2_30d	3

Table 14: Randomized Experiment Order: Solution 1/2, Layup L1/L2, Weathering Time 0/15 days

Randomized experiment order	Weathering series	ID of specimen
1	sol1_L1_15d	5
2	nonWeathered_L1	5
3	nonWeathered_L1	1
4	sol2_L1_15d	6
5	sol1_L1_15d	4
6	sol2_L1_15d	3
7	sol1_L1_15d	7
8	sol1_L1_15d	2
9	sol2_L1_15d	1
10	sol2_L1_15d	7
11	nonWeathered_L1	2
12	nonWeathered_L2	3
13	nonWeathered_L2	6
14	sol2_L1_15d	4
15	nonWeathered_L1	4
16	sol2_L1_15d	2
17	nonWeathered_L2	4
18	nonWeathered_L1	6
19	nonWeathered_L2	7
20	nonWeathered_L2	1
21	sol2_L1_15d	5
22	sol1_L1_15d	3
23	sol1_L1_15d	1
24	sol1_L1_15d	6
25	nonWeathered_L2	5
26	nonWeathered_L2	2
27	nonWeathered_L1	3

5 EXPERIMENTAL PROCEDURE

5.1 Weathering of Composite Materials

When speaking of weathering, in the following section this will be referred to as the complete immersion into a salt solution. Unlike the general weathering, including multiple degradation agents such as ultraviolet radiation and moisture, in this experiment the degradation mechanisms will be subject by focusing on a single degradation agent, seawater. For the weathering of the carbon fiber/epoxy panels, two 2l beakers are employed allowing the use of different concentrations of salt solutions. Furthermore, the size is chosen to fit at least 25 specimens simultaneously yielding a minimum spacing of 2mm between specimens (Fig. 8).

Consistent spacing between the specimens during exposure to the salt solution is accomplished with the assistance of cable tie. Eight strips of cable tie are arranged in a row on one cable tie strip of the same type. In this manner, the specimens can be positioned in the pockets of the cable tie. This arrangement is advantageous as it optimizes the available space while the surfaces of the composite material are still exposed to the surrounding salt water medium allowing full circulation. Sets of specimens are created according to the design of experiments. The simple rack construction can be expanded for more specimens by adding more cable ties.

In order to achieve a weathering set-up of accelerated lifetime testing the temperature of the internal salt solution needs to be increased above the service temperature of real-life applications. Moreover, the composite material possesses a glass transition temperature, a characteristic temperature where the mechanical

properties change drastically if exceeded. For the carbon fiber/epoxy material of this study the glass transition temperature is determined to be 86°C using dynamic scanning calorimetry (DSC) after curing. Hence, any elevated temperature that remains below this characteristic value can be used to perform accelerated weathering experiments. In this study, a weathering temperature of $T_w = 65°C$ is chosen.

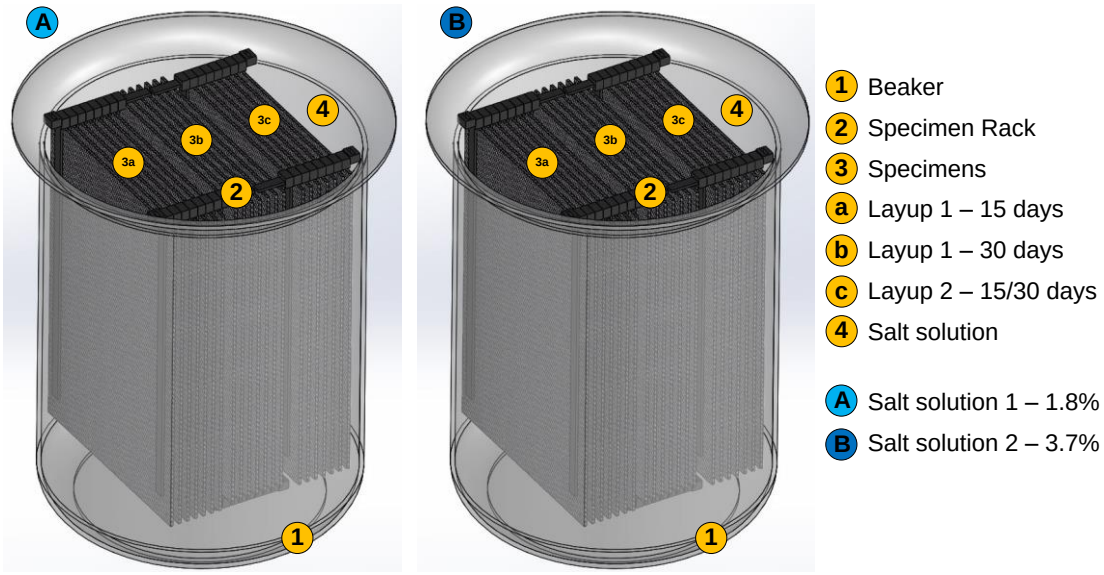

Fig. 8: Glass Beakers Containing Salt Solutions 1 (A) and 2 (B) with Rack and Specimens

A fully enclosed and insulated container around the beakers is needed to reduce temperature variability and evaporation. A double-walled tank is created by using two high-temperature polypropylene reservoirs which are different in size. The artificial boundary separates the immersion heaters in the outer tank from the salt solution in the beakers in the inner tank creating a secondary heat source (Fig. 9). Any contact of salt water with the immersion heaters could otherwise lead to a corrosion process and thus irretrievable damage to the weathering equipment. The outer tank is covered with a lid and fully insulated with a 5cm thick layer of moisture-venting polyurethane insulating

foam. An open-cell construction allows moisture to evaporate from this foam insulation. Material is heat resistant to a temperature up to 93°C (200° F). Two immersion heaters in the external tank keep the temperature of the deionized water steadily at 65°C for the full length of experimentation, lasting 30 days. The chosen immersion heaters are of the type Cole Parmer PolyScience LX Immersion Circulators. The maximum capacity of each heater is 20liters of fluid with a temperature range of ambient to 98°C. Temperature stability is ±0.07°C.

All material and equipment except the immersion heaters are chosen to be chemically resistant to salt solutions at elevated temperatures.

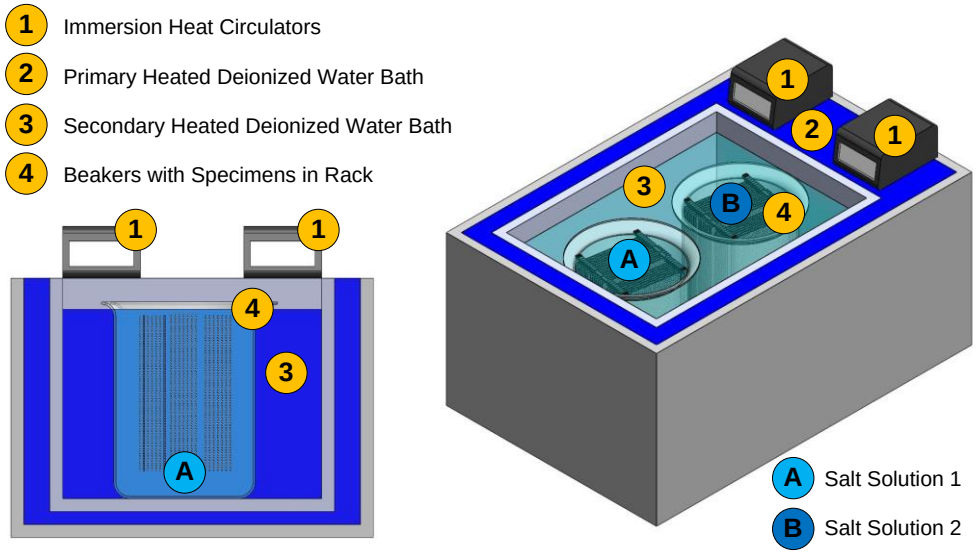

Fig. 9: Weathering Tank Cross-Section with Beakers and Specimens (left) and Isometric (right)

The salt solutions are prepared by dissolving crystalline sodium chloride in deionized water. The first solution holds 1.8 mass% of NaCl. The second one has 3.7 mass% of NaCl. A concentration of 3.7 mass% means that 1000g salt solution is composed by 3.7g of NaCl and 996.3g deionized water. The concentrations are checked once a week after insertion of the specimens by means of an optical salinity meter for

marine applications. This optical refractometer allows in situ salinity measurements in seawater (Fig. 10). There is also the ASTM standard D1141 [27] which describes a Standard Practice for the Preparation of Substitute Ocean Water. This substitute ocean water may be used for laboratory testing where a reproducible solution simulating sea water is required. Examples are for tests on oil contamination, detergency evaluation, and corrosion testing. Since the concentrations of ocean water varies depending on location the above mentioned method will be used instead. This reference shall show that ocean water usually contains a variety of inorganic salts. Nevertheless, sodium chloride holds the majority of influence on the ocean's salinity as Table 15 shows.

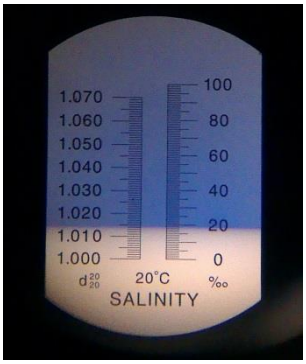

Fig. 10: Measurement of Salt Concentration with Optical Refractometer

Table 15: Extract of Chemical Composition of Substitute Ocean Water based on ASTM D1141

Compound	Concentration, g/L
NaCl	24.53
$MgCl_2$	5.20
Na_2SO_4	4.09
$CaCl_2$	1.16
KCl	0.695
$NaHCO_3$	0.201
KBr	0.101
H_3BO_3	0.027
$SrCl_2$	0.025
NaF	0.003

The non-weathered specimens are stored at an ambient temperature of 25°C and in humidity of around 50% - 70% while the other specimens are being weathered. As mentioned before, all specimens are desiccated in indicating silica gel to extract atmospheric moisture for a period of seven days before weathering or drop-weight testing. Subsequent to the description of weathering, the next sections covers the procedure of drop-weight testing.

5.2 Drop-Weight Impact Testing

The test method of drop-weight impact testing determines the strength and damage resistance of multidirectional composite material plates. A flat, rectangular composite specimen is subjected to an out-of-plane impact (perpendicular to the plane of the laminated plate) using a drop-weight tower equipped with a hemispherical impactor. Attached to the falling weight, the hemispherical striker tip with a diameter of 25.4 mm is connected to a dynamic load cell to measure impact load–time history. The test procedure compared to a quasi-static indentation test differs by the velocity of the impact event. The drop-weight impact machine and its used fixture are displayed in Fig. 11. The impact support fixture is designed to meet the standard ASTM standard D7136/D7136M [28]. The cut-out in the center of the fixture has dimensions of 76mm by 127mm. Four clamps restrain the specimen during impact with a holding capacity greater than 1100N.

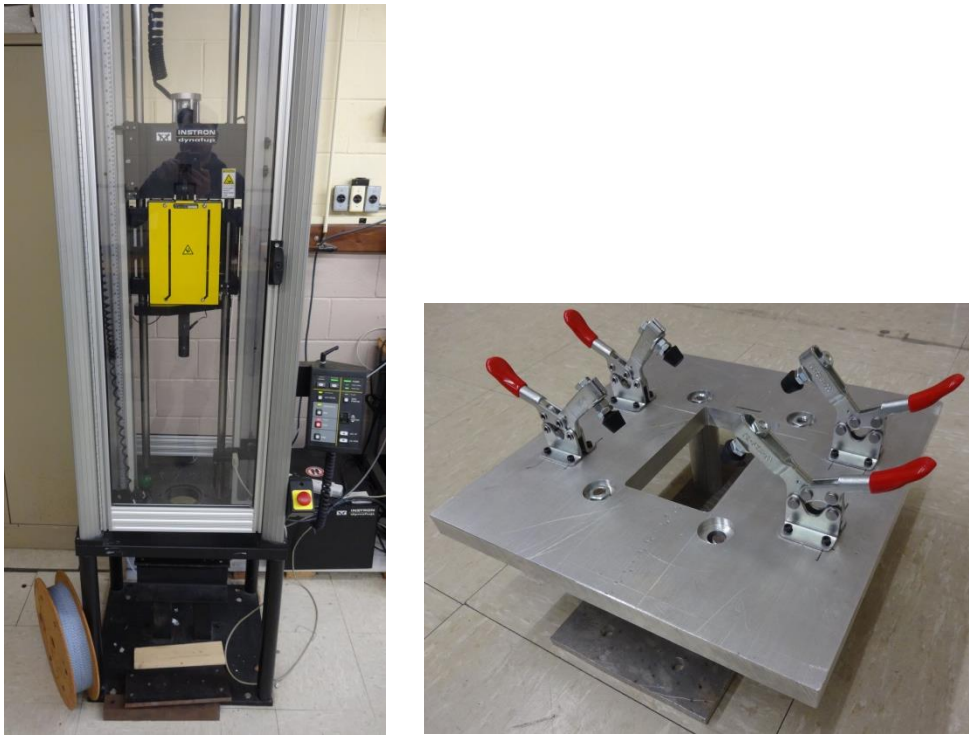

Fig. 11: Drop-Weight Impact Machine Instron Dynatup Model 9210 (left) and Fixture (right)

The potential energy of the drop-weight is a characteristic for this experiment and specified prior to testing. The potential energy is defined by mass and drop height of the impactor.

$$E = H\, m_d\, g \tag{13}$$

$$v_0 = \sqrt{2gH} \tag{14}$$

Where H is impactor drop height, m_d is impactor mass for drop height calculation, g is acceleration due to gravity, E is potential energy of impactor and v_0 is impact velocity. Due to friction and variability of impact drop height, the impact velocity v_0 is

determined with a conductive velocity flag apparatus right before the impact event for each drop-weight experiment.

In trial runs, the potential energy to see material failure was determined. One non-weathered drop-weight specimen was used for the trial run series and was impacted multiple times. The potential energy was increased gradually until material failure became visible starting with the minimum impactor mass of $m = 7.29kg$ and a drop height of $H = 120mm$. The drop height was increased by 20mm each trial step until a drop height of $H = 1100mm$ ranging from impact velocities of $v_0 = 1.44\frac{m}{s}$ to $v_0 = 4.49\frac{m}{s}$. Only by increasing the impactor mass, material failure could be observed externally. A new impactor mass of $m = 12.92kg$ at $H = 860mm$ was chosen, as the energy level is high enough to create damage on the composite material. According to equation (13) the potential energy of this set-up totals approximately 109J. The exact drop height can be found after each experiment by using the set zero function of the drop-weight testing machine. Five individual velocity tests are performed before any test series. The velocity measured by the velocity flag at impact averaged to $v_0 = 4.05\frac{m}{s}$.

5.3 Weathering Acceleration Method

5.3.1 Arrhenius Relationship and Effect of Temperature

The Arrhenius Relation can be used to relate a reaction of a given process to the temperature the components are exposed to. This relation is used in this study to relate the experimental submersion time of the composite specimens to the real-life service time. The Arrhenius equation governs the relation between accelerated weathering test and real time immersion:

$$k = Ce^{-\frac{E_a}{RT}} \tag{15}$$

where k is reaction rate constant, C is a constant, E_a is Activation Energy, R is the universal gas constant, T is absolute temperature.

Activation energy describes an energy barrier that must be surmounted by the reacting molecules before a reaction can occur. The activation energy is a constant for a material. At higher temperatures, more molecules enable diffusion reactions and lead to increased diffusion rates. The activation energy can be derived from different diffusion coefficients at various temperatures which equal an Acceleration Factor (AF). The AF relates the experimental temperature and time, to real-life service time at according service temperatures.

The diffusion characteristics of the composite material can be found using equations (4) and (5). Assuming that transversal diffusion follows the approximation of equation (10) the diffusion coefficient of the matrix D_m can be determined. Manipulating the Arrhenius Equation (6) into its logarithmic form, delivers equation:

$$\ln(D_m) = \ln(D_c) - \frac{E_a}{RT} \tag{16}$$

where D_m is the diffusion coefficient at absolute temperature T, D_c is a constant, $\mathrm{E_a}$ is Activation Energy, and R is the universal gas constant. A plot of $ln(D_m)$ against $\frac{1}{\mathrm{T}}$ yields a linear function with a slope that equals $-\frac{\mathrm{E_a}}{\mathrm{R}}$. R is generally known. Knowing the activation energy $\mathrm{E_a}$ the function for AF is completely described by equation (17):

$$AF = e^{\left(\frac{\mathrm{E_a}}{\mathrm{R}}\right)\left(\frac{T_2 - T_1}{T_1 T_2}\right)} \tag{17}$$

where T_2 equals the experimental test temperature in Kelvin and T_1 is the potential service temperature of the applied composite material that can be faced in real-life conditions. The AF can be manipulated by selecting a certain experimental and potential service temperature of the salt solution.

In order to describe the velocity of degradation, a separate study for finding the aforementioned diffusion coefficients is accomplished. Water saturation limits of the composite material plates are found in the diffusion study besides diffusion coefficients.

5.3.2 Diffusion Study

For the diffusion study, the weathered composite material specimens exposed to both salt solutions at 65°C (described in the prior sections) are studied. The same specimens including the material and dimensions that are tested dynamically are used for the diffusion study. For this reason, the diffusion study can be run up to the maximum weathering time of 30 days. Also, the same salt solutions are kept at 25°C as comparative diffusion series.

There were at least five specimens repetitively tested for each solution and temperature to ensure repeatability of the measurements. Fig. 8 displays the arrangement of the specimens in the diffusion study beakers with the cable tie rack. Throughout the duration of the experiment, the specimens were periodically removed from their beaker, dried with paper towel, weighed, and placed back in their respective beaker. At the point of replacing the specimens, they were all randomized in their position within the according set. Particularly, the two specimens facing the glass wall of the beakers should be exchanged due to the significantly increased gap to the specimens' surfaces. This procedure is part of the randomization technique described earlier to decrease the random error of the experiment. In the first 48 hours the specimens were weighed every 150 minutes. As the rate of diffusion into the composite material naturally decays, the intervals between mass measurements of the specimens are performed daily from the third day until the 15^{th} day, and weekly after the 15^{th} day.

The edges of the specimen are left uncovered so that diffusion could also happen through them. However, the total surface area of the edges compared to the total surface area of the specimen (compare Table 3) is less than 2%. Additional epoxy covering the cutting edges was not used because the post-curing of that epoxy could change the mechanical properties of the composite plates.

The relative mass increase $M(t)$ is reported for all specimens individually for the 65°C series as a function of time using equation (18). The maximum weight of 210g would be exceeded if all seven specimens of one set would be measured on the

precision Toledo scales (±0.5 mg). For the 25°C series the measurements are performed in sets of five specimens to lower the variability. Due to limited experimentation time, percent mass gain at saturation is obtained from the high temperature series to reach mass equilibrium. The low temperature series are continued to saturation, regardless of the weathering time interval. Total saturation is determined after specimens submerged in 65°C 1.8% and 3.7% salt solution displayed no mass gain for more than five days. All diffusion series reach a certain saturation level with different diffusion coefficients.

$$M(t) = \frac{m_t - m_0}{m_0} \tag{18}$$

where m_t and m_0 are sample mass at the time t and at the initial state, respectively.

6 RESULTS AND DISCUSSION

6.1 Results Diffusion Study

The point of saturation was found at 1.02% of the original mass for both layup 1 and layup 2. The diffusion coefficient is independent of the salt concentration as Fig. 12 shows for certain temperatures, 65°C and 25°C in this present study. The slower diffusion process at 25°C becomes apparent by the decreased slope of the diffusion curves.

Diffusion coefficients are presented in Table 16 for diffusion progress at 65°C and 25°C. According to the relative mass gain curves in Fig. 13, the t_{50} time at 65°C was reached after 34.4 hours, while 50% of saturation at room temperature was reached after 175 hours.

Table 16: Diffusion Characteristics of Accelerated Diffusion Series at 65°C and 25°C

Temperature T (°C)	Time t_{50} (h)	Diffusion Coefficient D_m (m²/s)
25	175.0	(2.70±0.06) E-12
65	34.4	(1.37±0.03) E-11

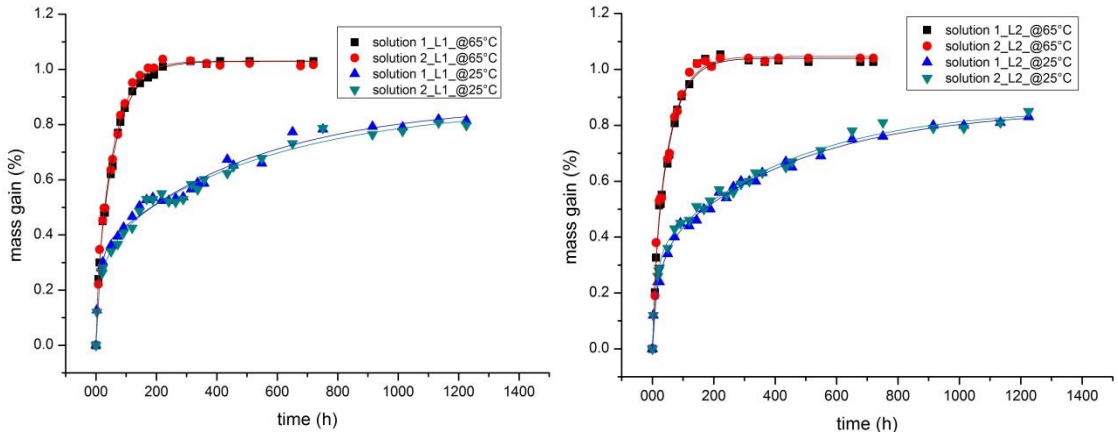

Fig. 12: Relative Mass Gain over Time of Layup 1 (left) and of Layup 2 (right)

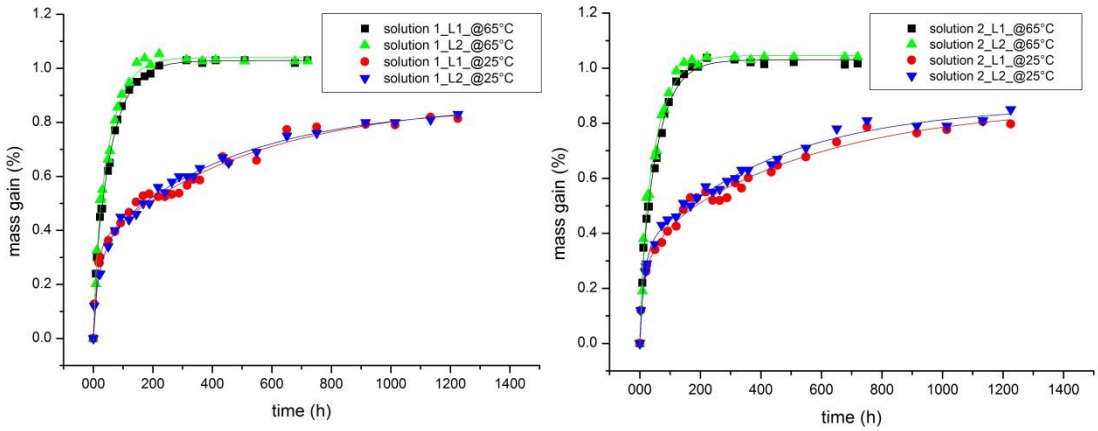

Fig. 13: Relative Mass Gain over Time in Solution 1 (left) and in Solution 2 (right)

Total saturation was obtained by the 65°C. Since all specimens, independent of temperature, reach the same equilibrium saturation, the diffusion of the 25°C samples was ended at 50 days. All diffusions series reached at least 50% saturation, to solve the Arrhenius equation (6) with t_{50}. R^2 greater than 98% was reached for the exponential fit functions in Fig. 12 and Fig. 13.

Knowing $t_{50,}$ the time until 50% of saturation is reached and the thickness of the specimens, the diffusion coefficient D was calculated according to equation (5). This diffusion equals the transversal trough-thickness diffusion rate D_t. Applying equation (8) with the determined fiber volume fraction f=55% gives an approximated ratio of the diffusion coefficient in the pure epoxy D_m to the measured diffusion measured transversal diffusion coefficient in the composite material.

$$D_m = \frac{31}{9} D_t \tag{19}$$

In Fig. 14 the natural logarithm of D_m is plotted over 1/Temperature and from the slope of the linear trend the activation energy can be extracted using equation (16).

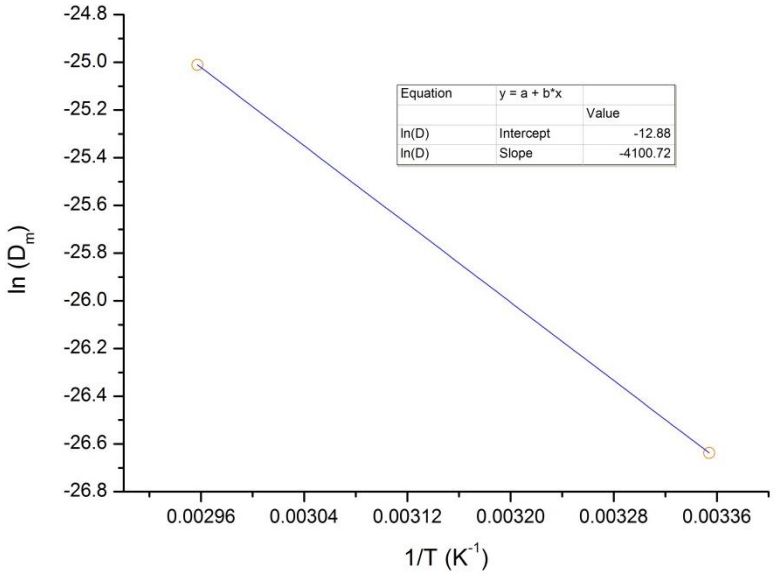

Fig. 14: Natural Logarithm of Diffusion Coefficient over Temperature^{-1}

The acceleration factors were found with equation (17) for the experimental submergence temperature of 65°C. The calculated acceleration factors range from 5 to 20, corresponding to service temperatures from 25°C to -2°C, respectively. Consequently, 30 days of experimental submergence at elevated temperature signify a real weathering time of 0.5 to 2 years of diffusion and concomitant degradation.

Relative thin specimen dimensions may be a reason for high diffusion ratios at both weathering temperatures. Moreover, the void content of the manufactured composite material may have accelerated the diffusion process significantly. The acceleration factors are consequently in a low range of simulated time.

6.2 Low Velocity Impact Response

Fig. 15 displays the schematic of a specimen fixed in the drop-weight fixture and subjected to an out-of-plane impact event by a hemispherical impactor. The load as a function of time is shown in Fig. 15 on the right.

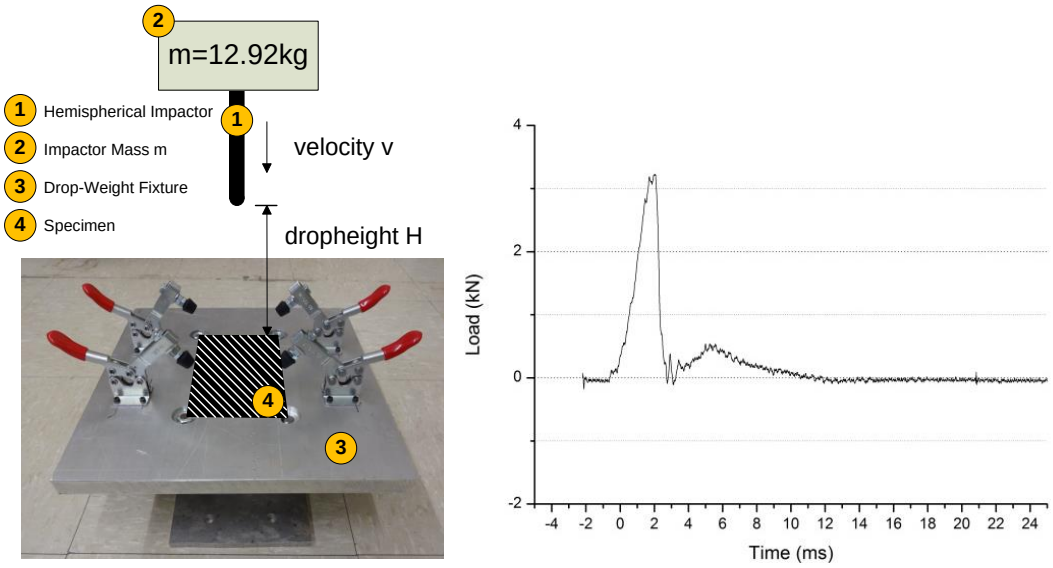

Fig. 15: Schematic Set-up of Drop-Weight Experiment (left) and Exemplary Load over Time Curve

The sequence of events happening during the experiment is described in the following. Prior to the drop-weight experiment, the impactor tip was positioned at the pre-defined height H=860mm above the specimen's surface holding impact mass of m=12.92kg in position. The drop-weight experiment was initiated by triggering the release mechanism at the drop-weight tower. The impactor was then accelerated by gravitational force towards the upper specimen's surface. The zero-point of the time was referenced as the moment of impact once the impactor hits the specimen possessing the impact velocity $v_0 \approx 4.05 \frac{m}{s}$. In this moment, the load immediately increased to find a maximum within 2ms. After reaching the peak load at a value of around 2.4kN to 3.1kN depending on the composite layup and weathering time, the curve suddenly dropped

before finding a second peak at a much lower level of around a tenth in magnitude. This sudden drop of the first peak reflects the elastic deformation and failure of the tested material. Short dips or not smooth parts in the load response indicate damage events such as debonding of fiber and matrix, delamination of the different plies, fiber breakage or matrix failure, and boundary effects. The crack propagation absorbed most of the energy before the failure process comes to a standstill. The second peak resulted from the saved energy and inertia of impactor still moving downwards. This time, elastic displacement was returned to the direction of impact resulting in a short increase of load. Moreover, the crack ends were expanded to the boundaries (supporting fixture area and clamps). Comparisons between the different load-time histories in the following sections show that it was not a rebound causing this second peak but the characteristics of the crack propagation. According to the graph, the second peak occurred within 4ms to 10ms after impact. Table 17 shows an overview of the first mean peak loads for the weathering series of both layup 1 and layup 2.

Table 17: Mean Peak Load Values of Studied Specimens, 95% Confidence Interval in Brackets

Series	Layup 1 - Mean Peak Load (kN)	Layup 2 - Mean Peak Load in (kN)
Non-weathered	2.71 [±0.16]	3.12 [±0.09]
Solution 1, 15 days	2.55 [±0.11]	2.93 [±0.21]
Solution 1, 30 days	2.65 [±0.07]	2.90 [±0.18]
Solution 2, 15 days	2.60 [±0.10]	2.57 [±0.21]
Solution 2, 30 days	2.42 [±0.11]	2.43 [±0.13]

6.2.1 Layup 1– Individual Impact Responses of Cross Ply Composites

The non-weathered cross ply layup L1 failed violently at approximately 2.71kN. All tested specimens showed similar magnitude before crack initiation and damage development (Fig. 16). The peak loads took place after around 1.7ms to 2.9ms after impact. The curves suddenly dropped before their second peaks at a level of around a tenth in magnitude of the first peak. Longitudinal cohesive cracks in the matrix mostly led to this type of failure. The rear view shows that there were barely through thickness cracks in the non-weathered specimens just local matrix and fiber failure in the impact region (Fig. 19). The load-time history of specimen #3 shows a slightly different behavior. A maximum load of only 2.34kN was reached before a second peak which was somewhat elongated like a plateau of 1.6kN occurs. This shows delayed failure which may be caused by the change of direction of the crack propagation visible in the post-mortem image (Fig. 19). For all displayed curves, the second peaks decayed after 10ms to reach the zero level.

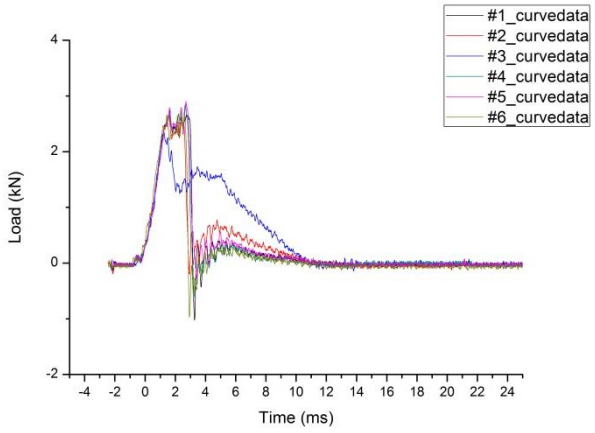

Fig. 16: Load-Time History: Layup L1 Non-Weathered Specimens

Quick drops after 3.3ms to 3.6ms lead to an oscillation of the load curve before leveling to zero. This behavior arises from the dynamic instrumentation and does not

reflect the actual load curve after passing the non-load state. These oscillating sections, especially the parts of negative values, do not represent the material's behavior and are therefore left out of analysis of the response.

The weathered specimens in solution 1 failed at lower peak loads than the non-weathered specimens (Fig. 17). The series of specimens tested after 15 days of salt water exposure showed a maximum impact-opposing force of around 2.55kN. Their peak loads all coincided on the same split second of 1.4ms after impact. The path of the downward slope differs in two characteristics. The majority (five of seven) of the specimens did not show a distinct second peak load while specimen #4 and #6 showed an elongated decay creating a second peak of the load at half of the initial peak magnitude. The curves eventually went back into the non-load condition after 12ms. The series of specimens tested after 30 days failed at a peak load of around 2.65kN which is marginally higher than the aforementioned series. The peak load lasted from millisecond 1.5 to 2.8ms.

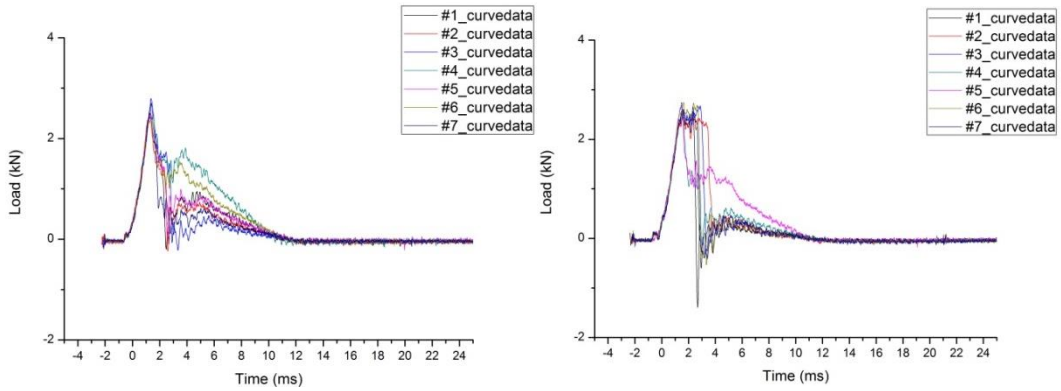

Fig. 17: Load-Time History: Layup L1 Weathered in Solution 1 for 15 days (left) and 30 days (right)

The specimens immersed in solution 2 burst at even lower loads than the non-weathered and the specimens placed in the low-salt solution 1 (Fig. 16 and Fig. 17). In average, the samples fail at 2.60kN after 15 days and at 2.42kN after 30 days of exposure (Fig. 18). Other than that, the 15 days series of solution 2 showed similar behavior as the 30 days series of solution 1. A fairly scattered pattern of load-time histories was recognizable for all data plots of the 30 days-weathered specimens in solution 2. Every curve displays the first peak load within 1.5ms and 2.3ms. The second peaks' magnitudes vary from eight tenth (specimen #1) to one tenth (specimen #3) of the first peak load. This behavior may be caused by the diffusion process and the concomitant weakening of the material. The material still failed catastrophically but less brittle. However, a consistent level of first peak loads allowed for further analysis.

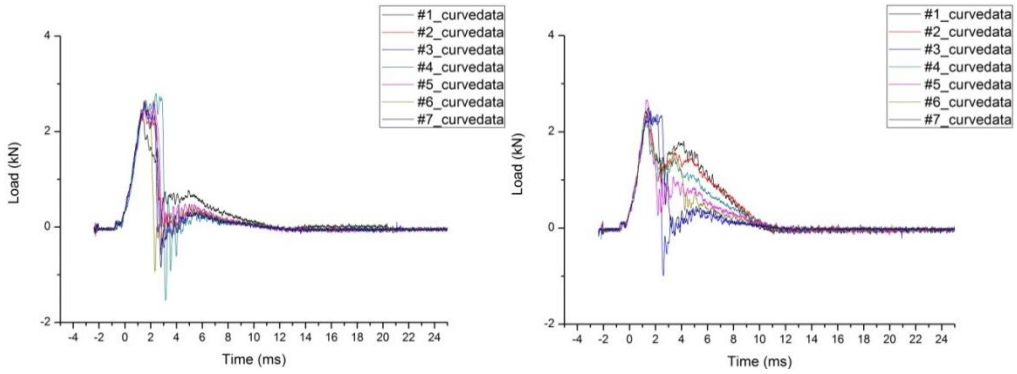

Fig. 18: Load-Time History: Layup L1 Weathered in Solution 2 for 15 days (left) and 30 days (right)

The post-mortem images in Fig. 21 display a greater damage area compared to the non-weathered specimen. Through-thickness cracks and delamination with subsequent chips of the outer plies are apparent. Moreover, cracks propagating towards the long edge of 30 days-weathered specimens both in solution 1 and 2 demonstrate a significant change of behavior. Alternating longitudinal cracks and fiber breakage zigzagged their

way through the specimen until the boundary was reached. This behavior is caused by the normal fiber orientation of the different plies. The crack followed these paths due to lower material resistance of the non-reinforced spots between fibers. Once the load is high enough, two parallel longitudinal cracks can bridge fibers by breaking them orthogonal to their orientation.

Post-mortem images of Layup L1

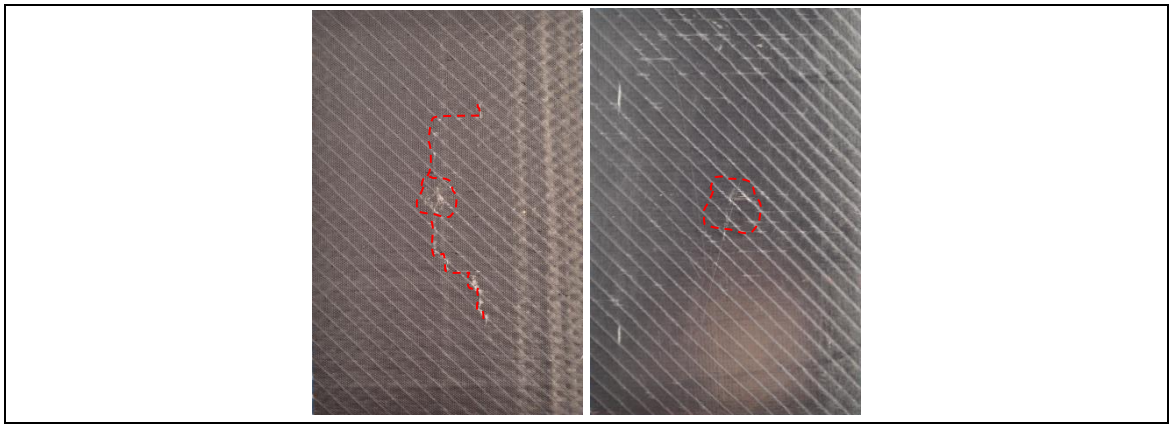

Fig. 19: Post-Mortem Non-Weathered, Specimen #3 (impact side on the left, back side on the right)

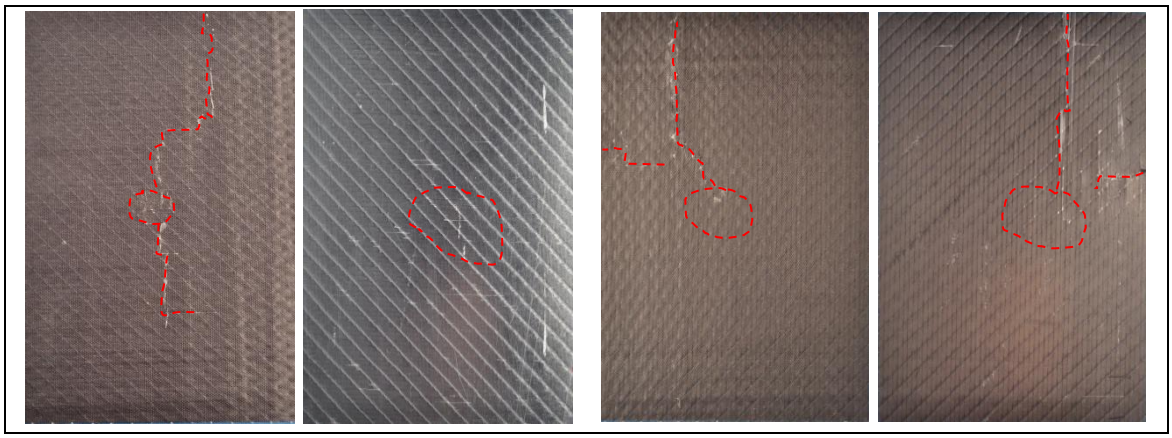

Fig. 20: Post-Mortem Specimen #4 (Solution 1/15 days) (left), #5 (Solution 2/15 days) (right)

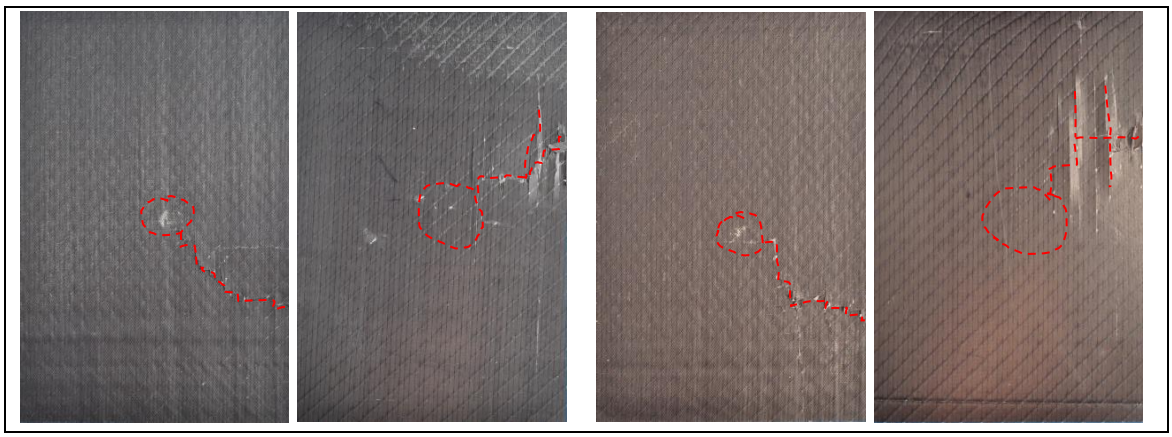

Fig. 21: Post-Mortem Specimen #7 (Solution 1/30 days) (left), #7 (Solution 2/30 days) (right)

6.2.2 Layup 2 – Individual Impact Responses of Angle Ply Composites

The non-weathered cross ply layup L2 failed violently at approximately 3.12kN. All tested specimens show similar magnitude before crack initiation and damage development (Fig. 22). The peak loads took place after around 1.9ms to 2.0ms after impact. The curves suddenly dropped before their second peaks at a level of around a tenth in magnitude of the first peak. Similar failure as with the non-weathered L1 specimens can be seen in Fig. 25. It is apparent, that the crack followed the fiber orientation. For layup 2, this means the crack spreads out from the impact area in an angle of ±45° compared to the long and short side of the specimens. The load-time histories of specimen #5 and #7, show elevated second peaks around 1.6kN and 2kN, respectively. This is seemingly caused by hindered crack propagation visible in the post-mortem image (Fig. 25). For all displayed curves, the second peaks decayed after 10ms to reach the zero level.

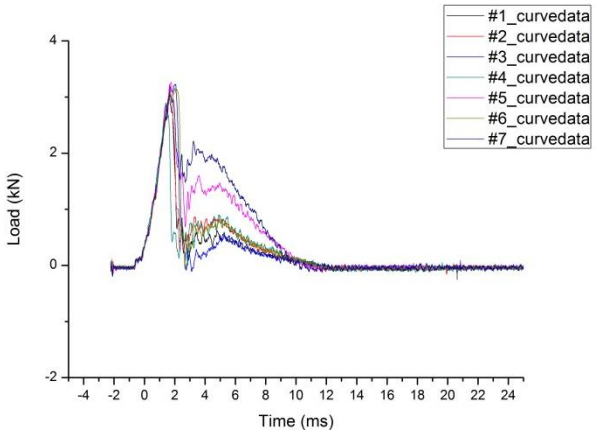

Fig. 22: Load-Time History of Non-Weathered Specimens Layup L2

The weathered specimens L2 in solution 1 failed at lower peak loads than the non-weathered specimens. The series of specimens tested after 15 days of salt water exposure showed an average peak load of around 2.93kN (Fig. 23). The failure of material happened around 2.2ms after impact. The majority of the specimens showed a second peak load at half of the initial peak load magnitude. The curves eventually returned into the non-load condition after 10ms. The series of specimens tested after 30 days failed at a peak load of around 2.90kN which is at a similar level as the specimens tested after 15 days. The peak load lasted from 1.7ms to 2.7ms after impact.

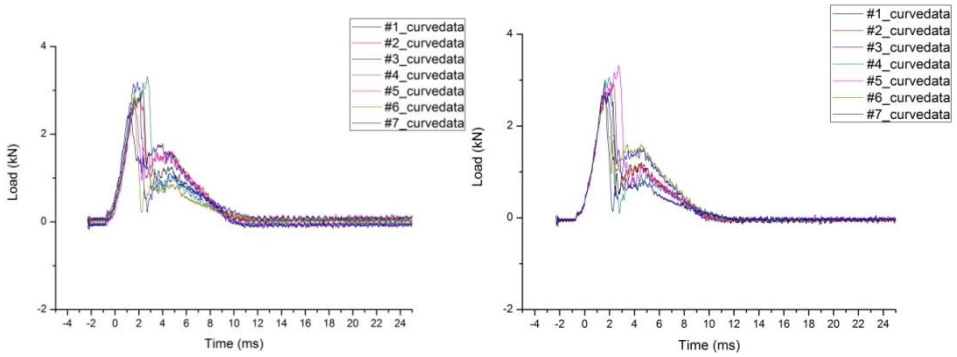

Fig. 23: Load-Time History: Layup L2 Weathered in Solution 1 for 15 days (left) and 30 days (right)

The specimens of layup 2 immersed in solution 2 failed at lower loads than the non-weathered and the specimens placed in the low-salt solution 1. In average, the samples failed at 2.57kN after 15 days and at 2.43kN after 30 days of exposure (Fig. 24). Every curve displayed the first peak load around 1.5ms except specimen #4. The second peaks' magnitudes totaled to half of the initial peak load magnitude. Through-thickness cracks and delamination with subsequent chips of the outer plies were apparent. Moreover, cracks propagating towards the long edge of 30 days-weathered

specimens both in solution 1 and 2 demonstrated a significant change of behavior. Alternating longitudinal cracks and fiber breakage zigzagged their way through the specimen until the boundary was reached. The post-mortem images (Fig. 27) display a greater damage area compared to the non-weathered specimen. The upper ply was partially separated. If this delamination is surrounded by transversal cracks, chips can come off the surface (third image from the left in Fig. 27).

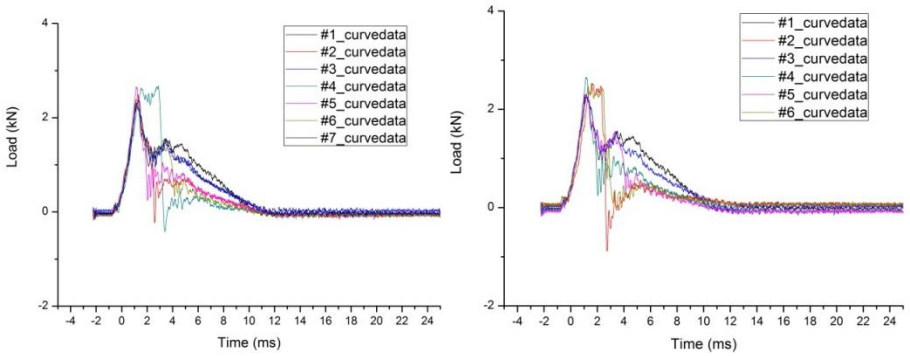

Fig. 24: Load-Time History: Layup L2 Weathered in Solution 2 for 15 days (left) and 30 days (right)

Post-mortem images of Layup L2

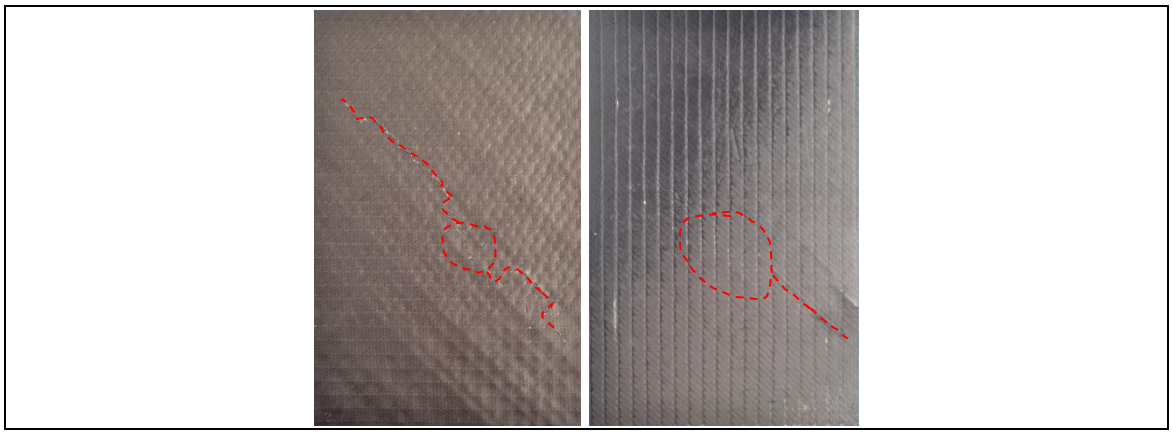

Fig. 25: Post-Mortem Non-Weathered, Specimen #5 (impact side on the left, back side on the right)

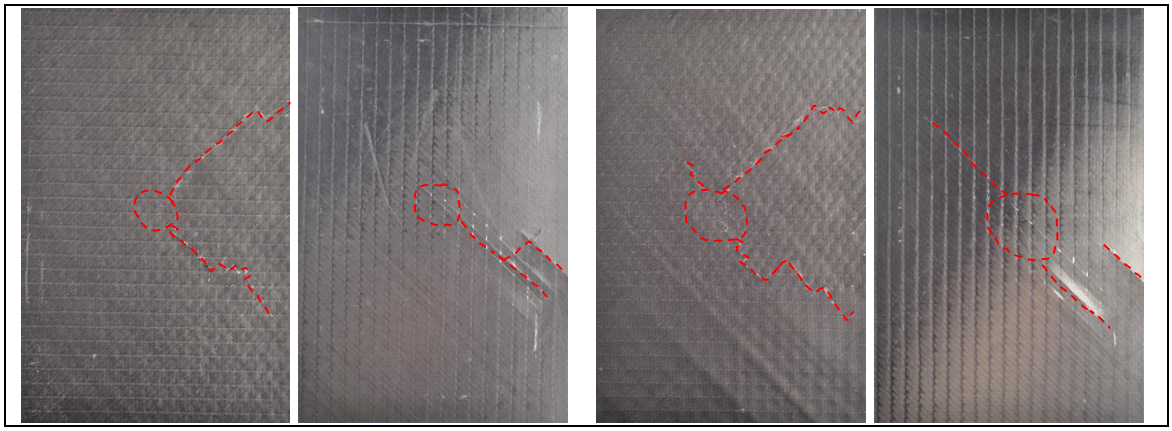

Fig. 26: Post-Mortem Specimen #7 (Solution 1/15 days) (left), #6 (Solution 2/15 days) (right)

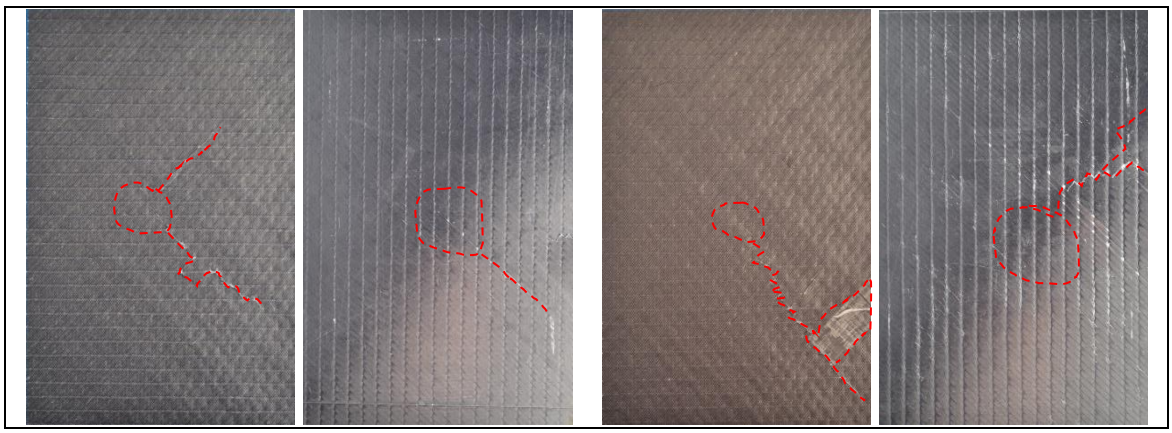

Fig. 27: Post-Mortem Specimen #5 (Solution 1/30 days) (left), #1 (Solution 2/30 days) (right)

Some of the weathered samples showed visible damage in the side view along the edges. These locations were examined to further inspect failure modes. Fig. 28 shows the cross section of a layup 2 sample subjected to 15 days of weathering in solution 1. The delaminated areas were apparent and visible by the horizontal cracks between the plies. In particular, the first and the fourth ply were subject of delamination. These were the two plies that were pre-manufactured in the bi-axial fabric and loosely stitched together before the epoxy infusion. Contrary to this, the center line of the four layers was not delaminated but bridged by transversal through thickness cracks through matrix and fibers. The length of damage concerned approx. 55mm of the edges. Moreover, all typical failure modes of an impacted composite material could be observed, such as delamination, cohesive and adhesive fractures, longitudinal and transversal cracks, fiber fracture and resin fracture.

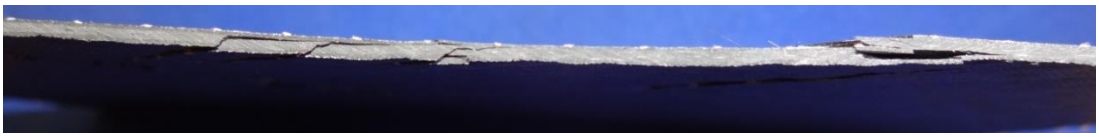

Fig. 28: Interlaminar Cracks/Delamination, Side View Specimen #1, (Layup 2/Solution 1/15 days)

6.3 Statistical Evaluation

In the following sections, the gathered data is being analyzed with the help of Analysis of Variance using probability plots, residual plots, main effect and interaction effect analysis as well as the pairwise comparison Tukey-Kramer test. The response Peak Load of the performed drop-weight experiments (Fig. 29 and Fig. 30) is basis of the following consideration and discussion.

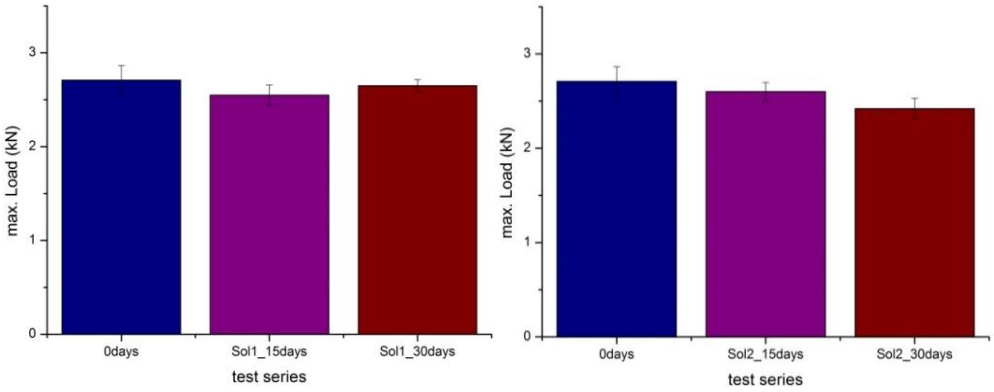

Fig. 29: Peak Loads: All Weathering Times of Layup 1 in Solution 1 (left) and Solution 2 (right)

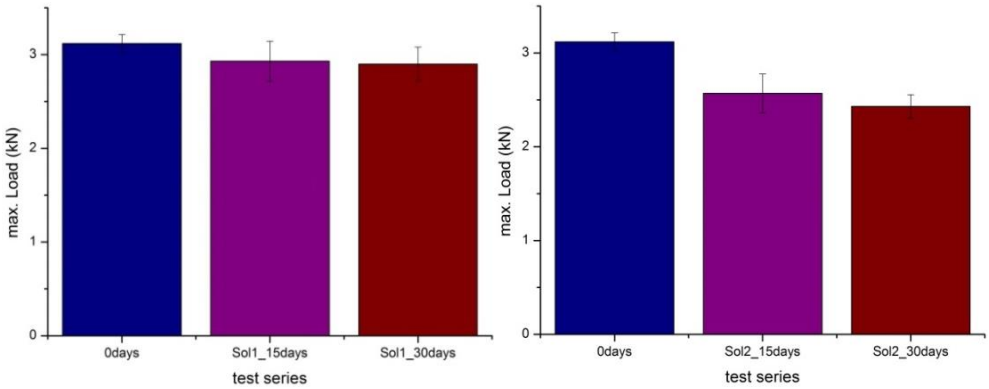

Fig. 30: Peak Loads: All Weathering Times of Layup 2 in Solution 1 (left) and Solution 2 (right)

The statistical analysis was performed in three steps (1), (2) and (3) (compare Fig. 31). The focus of factors was systematically shifted in each of the three steps. The first main factor solution with two concentrations and the second main factor weathering time with three different time spans and the blocking factor layup with two settings

were initially considered. Within the first two steps (1) and (2) the results of both solutions were examined individually. This allowed for comparison of the influence of the weathering time, particularly a potential change of the response between non-weathered and weathered specimens and checking the diversity of the blocking factor layup for each saline solution. The third step (3) focused on the comparison of the actually weathered specimens, the influence of the salinity and a possible interaction between these two main factors. Therefore, only two levels of the factor weathering time (15 days and 30 days) were taken into account for this third approach leaving out the non-weathered stage. This time, both levels of salinity and the blocking factor layup were compared as well as their interaction. The three-step approach for the performed experiments was chosen due to the fact that the weathered levels could only be assigned to each salinity level whereas the specimens of the non-weathered stages obviously had not been exposed to any solution.

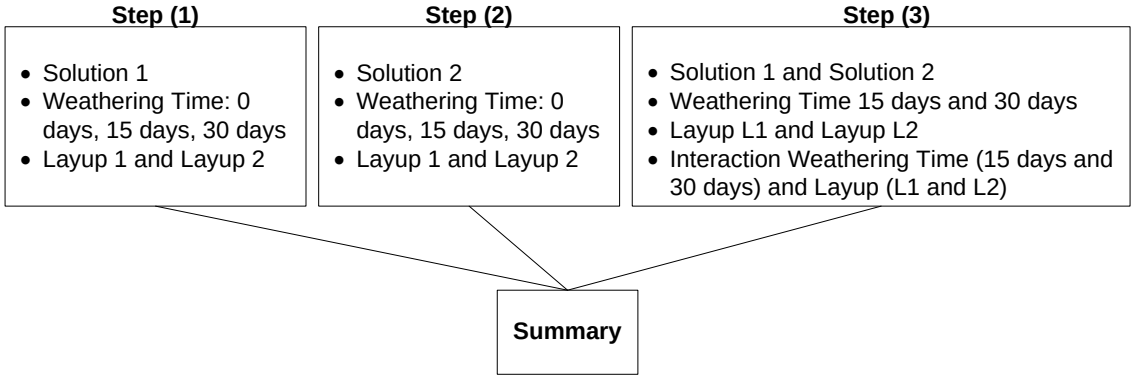

Fig. 31: Strategic Statistical Analysis in Three Steps

According to the developed model an Analysis of Variance (ANOVA) was performed for the main factors, the interaction and the blocking factor. The considered terms of the model in each of the three steps were applied accordingly, see equation

(12). For this purpose, the statistical software Minitab 17 was used. The significance level was chosen with a value of α=0.05.

6.3.1 Step (1) - Solution 1

In the first step (1) the response peak load was examined depending on the variables layup, weathering time for weathered specimens in solution 1. The ANOVA Table 18 shows all interesting components for the analysis. The first column describes the sources of variation including variation between the treatments, the error term and the total variation (total sums of squares).

The ANOVA underlies the following reduced model, compare equation (12):

$$y_{ijkl} = \mu + \tau_i + \beta_j + \delta_k + \epsilon \tag{20}$$

with $i = \{1,2,3\}; j = \{1\}; k = \{1,2\};\ l = \{1,2,3,\dots,7\}$

Table 18: ANOVA of Factors: Layup and Weathering Time (Step 1) for Solution 1

Source of Variation	DF	Adj SS	Adj MS	F-Value	P-Value
Layup	1	1.14179	1.14179	28.39	0.000
Weathering Time	2	0.31410	0.15705	3.91	0.029
Error	37	1.48783	0.04021		
Total	40	2.90323			

where DF is degrees of freedom, F test statistic, MS mean squares and SS sums of squares

It is apparent that the factor weathering time with p=0.029 has a significant influence on the response. Furthermore, the blocking factor layup holds a highly significant value of p=0.000. In the following overview the treatment coefficients are shown (Table 19). Treatment coefficients describe quantitatively the either positive or

negative effect of the level of each treatment on the response. Within one treatment the treatment coefficients' sum must equal zero because the coefficient for a factor level is the difference between the mean for that level and the overall mean. For that reason, having only two levels as it is the case for the blocking factor layup and having equal sample sizes, the level effect will be equal in magnitude because the mean is exactly in the middle (0.167 kN). The biggest stake in the factor weathering time holds the first level non-weathered stage (0.124kN).

Table 19: Treatment Coefficients of Factors: Layup and Weathering Time (Step 1)

Term	Coefficient	SE Coefficient	T-Value	P-Value
Constant	2.8198	0.0313	89.95	0.000
Layup				
L1	-0.1670	0.0313	-5.33	0.000
L2	0.1670	0.0313	5.33	0.000
Weathering Time				
0 days	0.1238	0.0449	2.76	0.009
15 days	-0.0794	0.0440	-1.80	0.080
30 days	-0.0444	0.0440	-1.01	0.320

where SE Coef is standard error of the coefficient, T test statistic

Main effect plots are used to examine differences between level means for one or more factors. There is a main effect when different levels of the factors weathering time, solution and layup affect the response Peak Load differently. Main effect plots are particularly helpful to see the direction of impact that factors cause. In the following main effects plot for the response Peak Load (Fig. 32), it becomes apparent that all factors affect the Peak Load in the experiments because the connecting lines between the level mean values possess a slope that is unequal to zero. The steeper the slope of the line, the greater the magnitude of the main effect. The factor weathering time has a

negative trend between the response of non-weathered and the ones weathered for 15 days. Nevertheless, the weathering time has a visibly lower and positive slope between the second and third level. The Tukey test in Fig. 33 shows the marginal significance of the pairwise compared weathering time levels 0 days – 30 days and 0 days – 15 days. Moreover, it is apparent that the difference of means between weathering time levels 15 days – 30 days are not significantly different. For that reason, the difference of the levels effect of the factor weathering time will be adressed in step (3) where the response of exclusively weathered specimens is subject of interest. With regards to the layup, the bi-axial angle-ply layup L2 shows better results than the simple cross-ply layup L1.

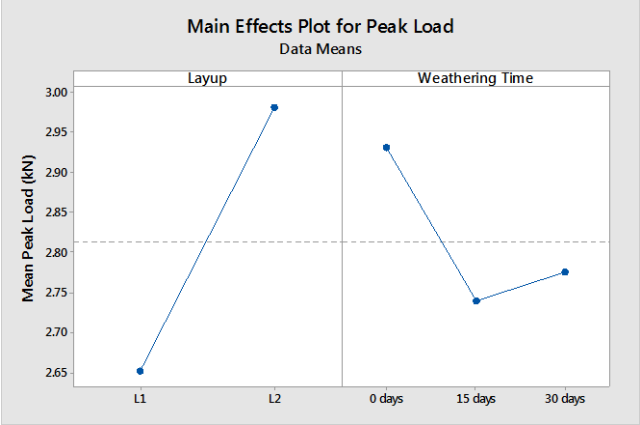

Fig. 32: Main Effects Plot for Peak Load in Step (1)

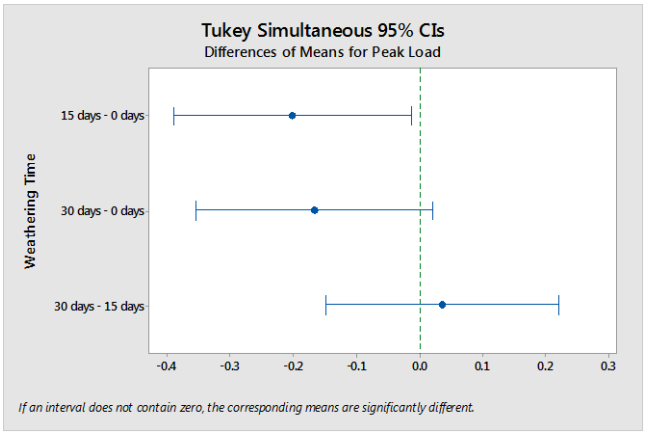

Fig. 33: Tukey's Test Results for Factor Weathering Time in Step (1)

The residuals of the response Peak Load for both factors weathering time and layup show equal magnitudes, respectively, which indicate equal variances. The residuals plots for the fits and the observation order all show random patterns (Fig. 34 and Fig. 35). The residuals plot for the response shows an upward trend. That means, for higher peak loads the error increases with positive values whereas low peak loads show increasing negative residual values. Hence, the normal distribution of the residuals is checked in Fig. 36. According to the distribution, all observations are situated within the 95% confidence interval of the normal distribution, thus the data points can be considered normal.

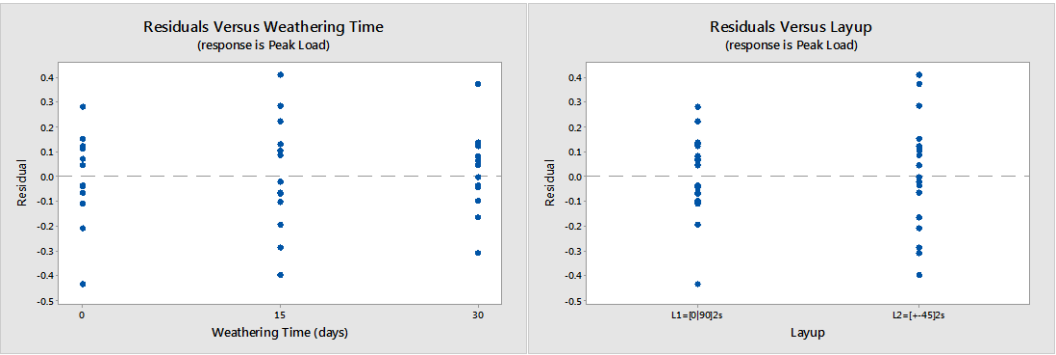

Fig. 34: Residuals Plot Weathering Time (left) and Layup (right) – Step (1)

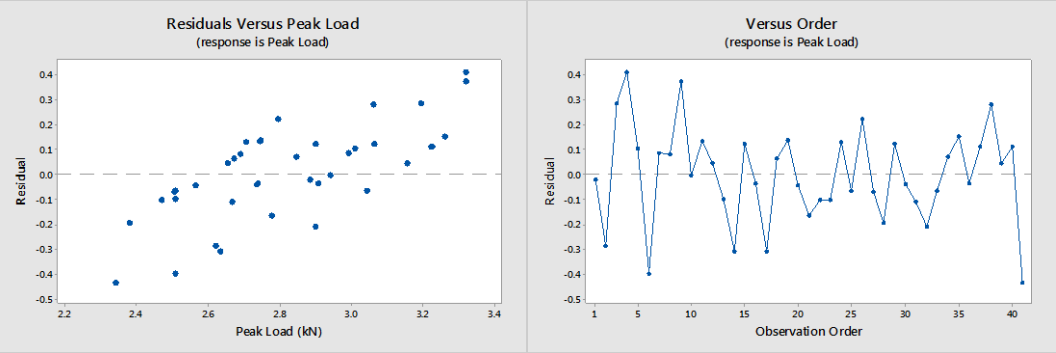

Fig. 35: Residuals Plot Peak Load (left) and Observation Order (right) – Step (1)

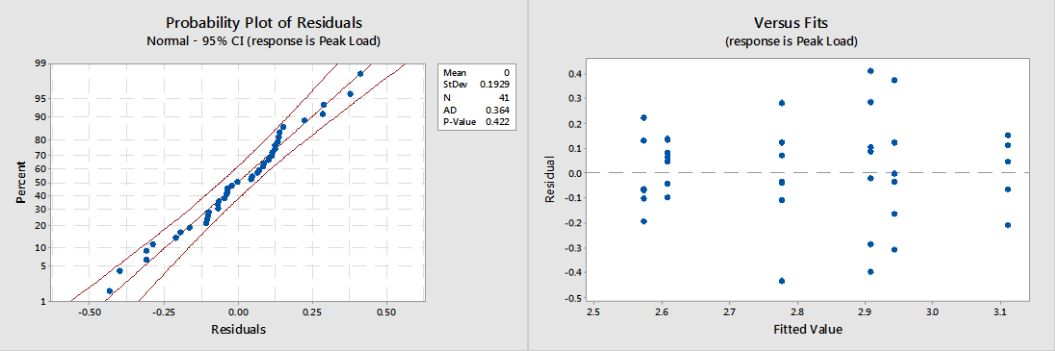

Fig. 36: Probability Plot with Confidence Interval of 95% and Residual Fits Plot - Step (1)

6.3.2 Step (2) - Solution 2

In the second step (2) the response Peak Load is examined depending on the variables layup, weathering time for weathered specimens in solution 2. The ANOVA Table 20 shows the fundamental components for the analysis.

The according ANOVA model is shown in the following:

$$y_{ijkl} = \mu + \tau_i + \beta_j + \delta_k + \epsilon \tag{21}$$

with $i = \{1,2,3\}; j = \{2\}; k = \{1,2\};\ l = \{1,2,3,\dots,7\}$

Table 20: ANOVA of Factors: Layup and Weathering Time (Step 2) for Solution 2

Source of Variation	DF	Adj SS	Adj MS	F-Value	P-Value
Layup	1	0.1366	0.13655	3.15	0.085
Weathering Time	2	1.7533	0.87663	20.20	0.000
Error	36	1.5626	0.04340		
Total	39	3.4448			

where DF is degrees of freedom, F test statistic, MS mean squares and SS sums of squares

Where DF is degrees of freedom, F is test statistic, MS is mean squares and SS is sums of squares.

The ANOVA table for this case shows strong significance of the factor weathering time with p=0.000 on the response. On the other hand, the blocking factor layup holds only a marginal significant value of p=0.085 which is obviously weaker than the result shown earlier for solution one. A potential difference in deterioration depending on the salt content of the weathering solution may be inferred from that fact. This point will be further discussed in the course of work.

The treatment coefficients for step (2) show the above mentioned phenomena (Table 21). The weathering time, especially Level 1 and 3 (0 days and 30 days), mainly

influence the response with 0.286kN and 0.221kN in opposing directions. The treatment coefficients of both layup types and the second level of weathering time, drastically shrink to absolute values less than 0.065kN.

Table 21: Treatment Coefficients of Factors: Layup and Weathering Time (Step 2)

Term	Coefficient	SE Coefficient	T-Value	P-Value
Constant	2.6497	0.0330	80.28	0.000
Layup				
L1	-0.0585	0.0330	-1.77	0.085
L2	0.0585	0.0330	1.77	0.085
Weathering Time				
0 days	0.2855	0.0469	6.09	0.000
15 days	-0.0644	0.0461	-1.40	0.171
30 days	-0.2212	0.0469	-4.71	0.000

where SE Coef is standard error of the coefficient, T test statistic

In the following main effects plot for the response Peak Load (Fig. 37) it is visible to what extent the factors weathering time and layup affect the Peak Load in the experiments weathered in solution 2. The factor weathering time has a negative trend between the response of non-weathered, weathered for 15 days and specimens weathered for 30 days. The Tukey test in Fig. 38 shows the significance of the pairwise compared weathering time levels 0 days – 30 days and 0 days – 15 days. However, it is apparent that the difference of means between weathering time levels 15 days – 30 days are not significantly different for this solution 2, similarly as shown for solution 1. For that reason, the difference of the levels' effect of the factor weathering time will be adressed in step (3) where the response of exclusively weathered specimens is subject of interest. The bi-axial angle-ply layup L2 shows better results than the simple cross-ply layup L1 at a gentle slope.

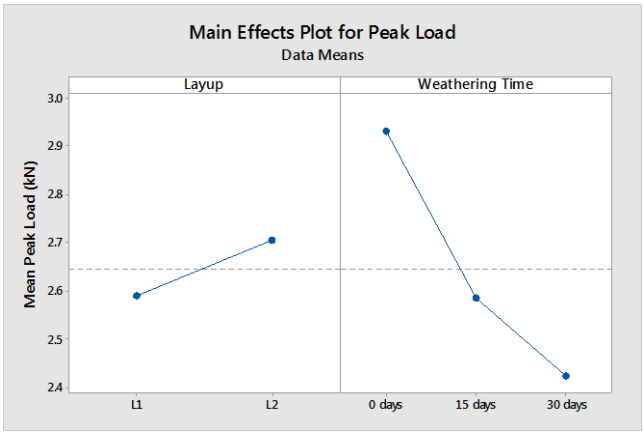

Fig. 37: Main Effects Plot for Peak Load in Step (2)

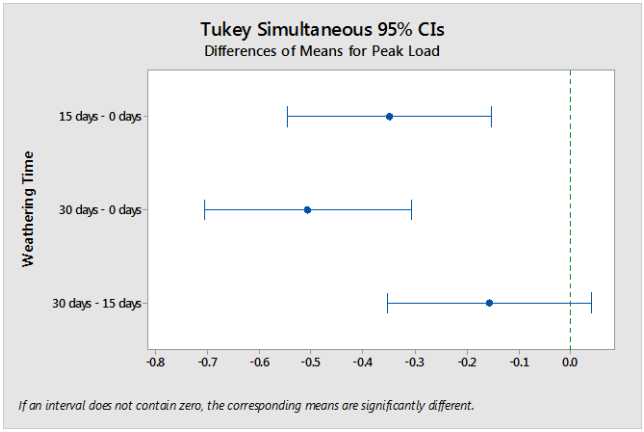

Fig. 38: Tukey's Test Results for Factor Weathering Time in Step (2)

The residuals of the response Peak Load for both factors weathering time and layup show equal magnitudes, respectively, which indicate equal variances (Fig. 39). The residuals plots for the fits and the observation order all show random patterns (Fig. 40 and Fig. 41). The residuals plot for the response shows a similar upward trend as seen before. This issue is only addressed for the sake of completeness. The normal distribution of the residuals may be observed in Fig. 41. According to the distribution, all observations are situated within the 95% confidence interval of the normal distribution, thus the data points can be considered normal.

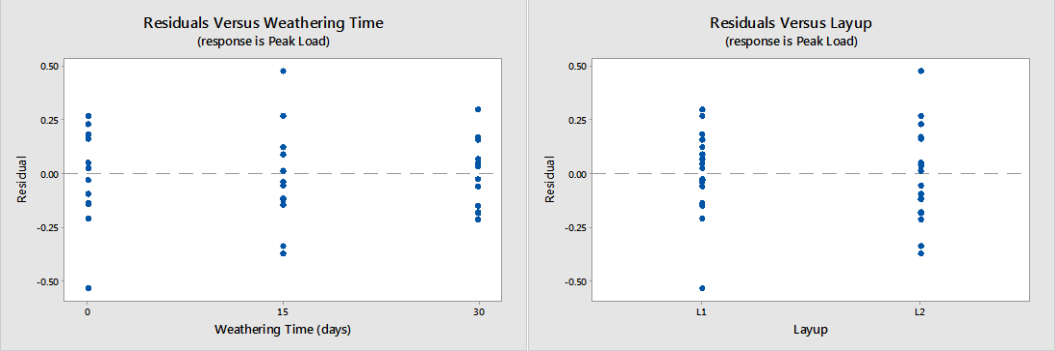

Fig. 39: Residuals Plot Weathering Time (left) and Layup (right) - Step (2)

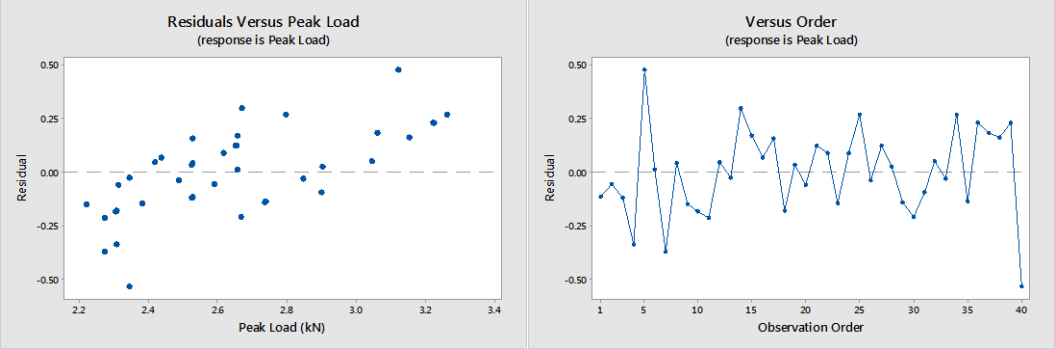

Fig. 40: Residuals Plot Peak Load (left) and Observation Order (right) - Step (2)

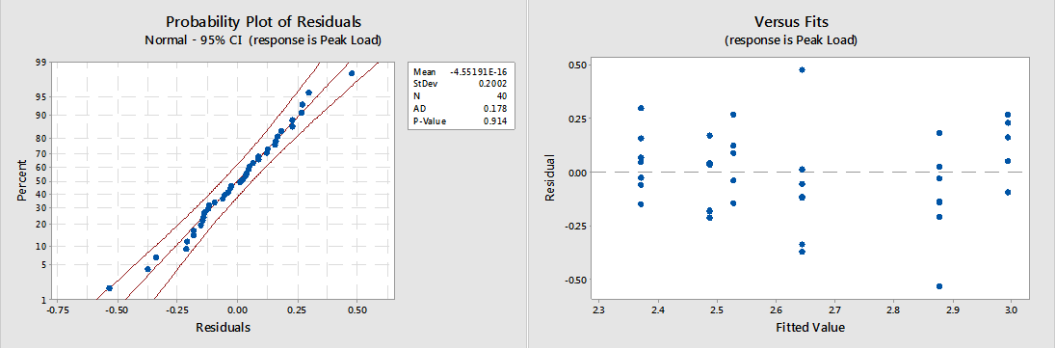

Fig. 41: Probability Plot with Confidence Interval of 95% and Residual Fits Plot - Step (2)

6.3.3 Step (3) - Weathering Experiments Exclusively

As mentioned before, in this third step of statistical analysis, the comparison of different weathering times is the main concern. Prior to this, both individual approaches of examining the solutions showed significance for the response. This time, the influence of the salinity and a possible interaction between the weathering time and the salinity are of interest.

The according ANOVA based on the original model is shown in the following:

$$y_{ijkl} = \mu + \tau_i + \beta_j + (\tau\beta)_{ij} + \delta_k + \epsilon \tag{22}$$

with $i = \{1, 2\}; j = \{1, 2\}; k = \{1, 2\};\ l = \{1, 2, 3, \dots, 7\}$

Note, that the factor weathering time with levels i only comprises $i = 1$ (15 days) and $i = 2$ (30 days) for the assessment in step (3).

The ANOVA Table 22 for this case shows a strong non-significance of the factor weathering time with p=0.301 on the response. Given that, one can deduct that the means of the weathering stages 15 days and 30 days are not significantly different. Furthermore, it is apparent that the factor solution has a strong influence on the Peak Load which means that the salt content does have a big impact on how the tested material responds. The p-value for the treatment solution ends up being p=0.000. As expected, the blocking factor layup holds a significant value of p=0.009. The interaction of weathering time and solution was found to be only marginally significant, with p=0.105.

Table 22: ANOVA of Main Factors and Interaction

Source of Variation	DF	Adj SS	Adj MS	F-Value	P-Value
Layup	1	0.33363	0.33363	7.33	0.009
Weathering Time	1	0.04971	0.04971	1.09	0.301
Solution	1	0.85974	0.85974	18.88	0.000
Weathering Time * Solution	1	0.12429	0.12429	2.73	0.105
Error	50	2.27642	0.04553		
Total	54	3.65474			

where DF is degrees of freedom, F test statistic, MS mean squares and SS sums of squares

The treatment coefficients for step (3) approve of the according ANOVA results. With regards to the solution, the treatments bring about a significant change of means by an absolute value of 0.125kN per level. However, the treatment effects of the weathering time are insignificantly low with 0.030kN.

Table 23: Treatment Coefficients of Main Factors and Interaction (Step 3)

Term	Coefficient	SE Coefficient	T-Value	P-Value
Constant	2.6328	0.0288	91.44	0.000
Layup				
L1	-0.0779	0.0288	-2.71	0.009
L2	0.0779	0.0288	2.71	0.009
Weathering Time				
15 days	0.0301	0.0288	1.04	0.301
30 days	-0.0301	0.0288	-1.04	0.301
Solution				
1	0.1251	0.0288	4.35	0.000
2	-0.1251	0.0288	-4.35	0.000
Weathering Time * Solution				
15 days * solution 1	-0.0476	0.0288	-1.65	0.105
15 days * solution 2	0.0476	0.0288	1.65	0.105
30 days * solution 1	0.0476	0.0288	1.65	0.105
30 days * solution 2	-0.0476	0.0288	-1.65	0.105

where SE Coef is standard error of the coefficient, T test statistic

The residuals of the response Peak Load for all factors weathering time, solution and layup show similar magnitudes, respectively, which indicate equal variances (Fig. 42 and Fig. 43). The residuals plots for the fits and the observation order all show random patterns Fig. 44 and Fig. 45. The residuals plot for the response shows a similar upward trend as seen before. Again, the normal distribution of the residuals is checked in Fig. 45, according to which the data points follow the normal distribution within 95% confidence interval.

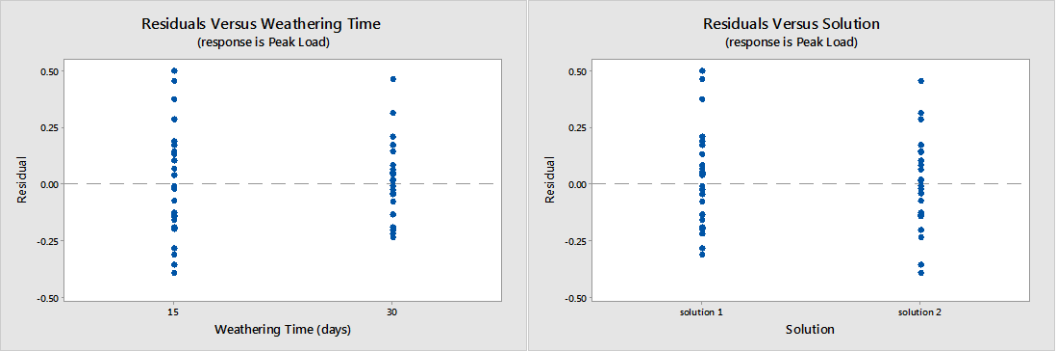

Fig. 42: Residuals Plot Weathering Time (left) and Solution (right) - Step (3)

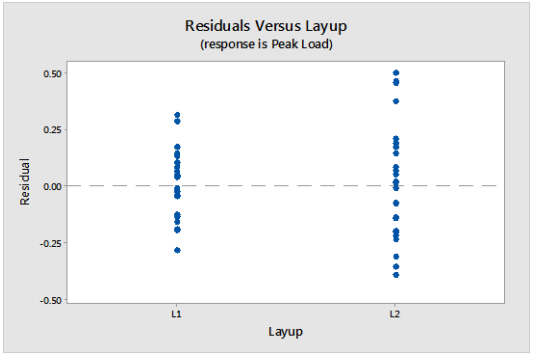

Fig. 43: Residuals Plot Layup - Step (3)

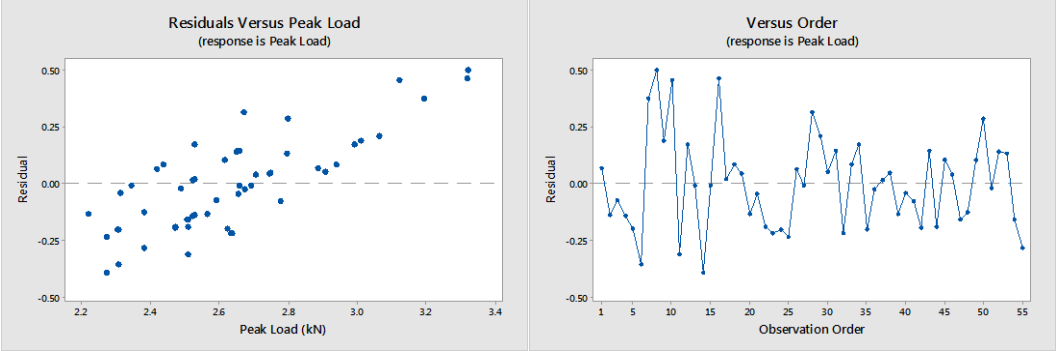

Fig. 44: Residuals Plot Peak Load (left) and Observation Order (right) - Step (3)

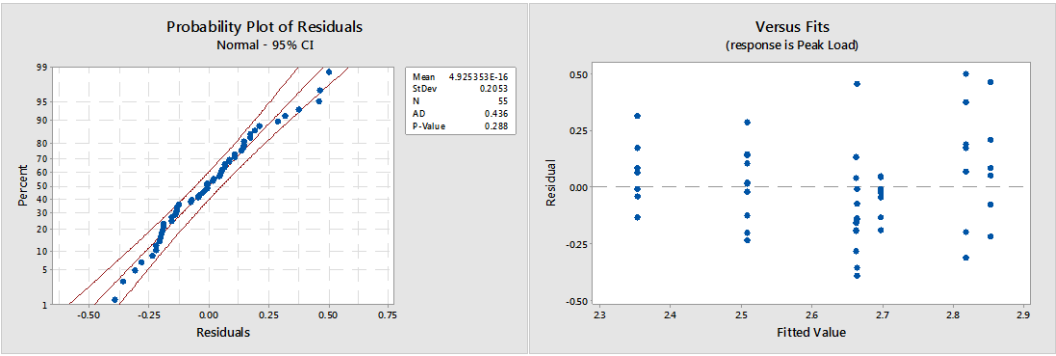

Fig. 45: Probability Plot with Confidence Interval of 95% and Residual Fits Plot - Step (3)

Main effect plots are used to examine differences between level means for one or more factors. There is a main effect when different levels of the factors weathering time, solution and layup affect the response Peak Load differently. Main effect plots are particularly helpful to see the direction of impact factors have. In the following graph for Peak Load (Fig. 46), it becomes apparent that all factors affect the Peak Load in the experiments because the connecting lines between the level mean values possess a slope unequal to zero. The steeper the slope of the line, the greater the magnitude of the main effect. The weathering time not only has a visibly lower slope but is also not significant as shown by the ANOVA results before. The plot for solution at level 2 indicates a decrease of the Peak Load for higher salt concentrations. With regards to the layup, the bi-axial angle-ply layup L2 shows better results than the simple cross-ply layup L1. The

interaction between the factor solution and weathering time is only marginally significant. In the interaction plot (Fig. 47) it is illustrated that the peak load for both weathering times in solution 1 are equal. There is a similar decrease of the peak load when specimens are exposed to solution 2. Less immersion time (15 days) shows a smaller decrease of the peak load mean than 30 days.

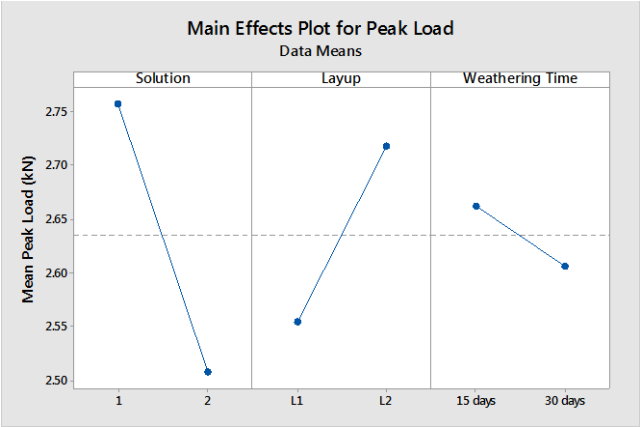

Fig. 46: Main Effects Plot for Peak Load in Step (3)

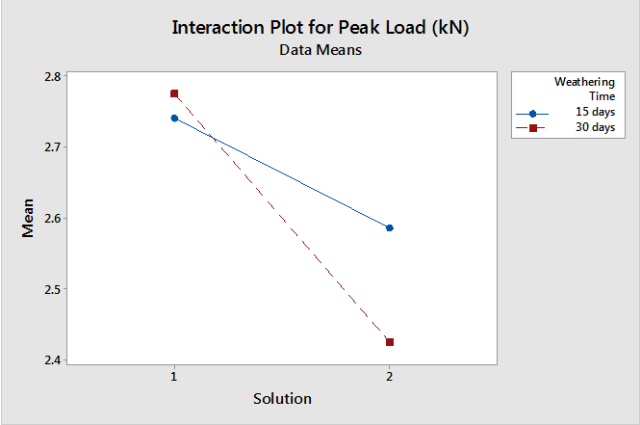

Fig. 47: Interaction Plot for Peak Load in Step (3)

Pairwise Comparisons

Eventually, a pairwise comparison between the factor combinations is performed in order to illustrate the found results. In Fig. 48 an interval plot with a 95% confidence

interval (CI) for the Peak Load mean is shown. The similar means for each layup pair regardless of the weathering time are conspicuous. For solution 1, L1 holds a mean of around 2.6kN where L2 holds a mean of approx. 2.9kN. Interestingly, this difference of both layups vanishes at the higher salt concentration of solution 2. The means are insignificantly different for weathering time of 15 days and 30 days around 2.5kN. This also means a drop in the total mean between solution 1 and solution 2. Additionally, the Tukey pairwise comparison test is performed to show grouping information for each factor using a 95% confidence interval.

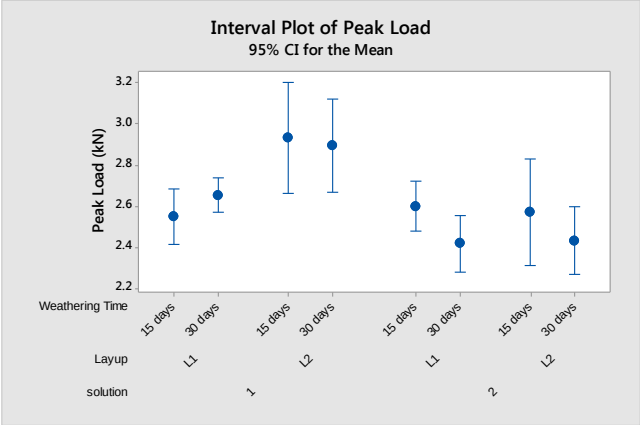

Fig. 48: Interval Plot for Main Factor Combinations in Step (3)

Regarding the layup, L2 holds the higher mean of 2.710kN compared to L1. Fig. 49 displays the found CI for the factor layup of CI=(0.040kN, 0.272kN). Regarding the solution, solution 1 holds the higher mean of 2.758kN compared to solution 1 (2.508kN). Fig. 49 displays the found CI for the factor solution of CI=(-0.366kN, -0.135kN). The insignificance of the factor weathering time in this step (3) of the statistical analysis is proved by Fig. 50 containing zero.

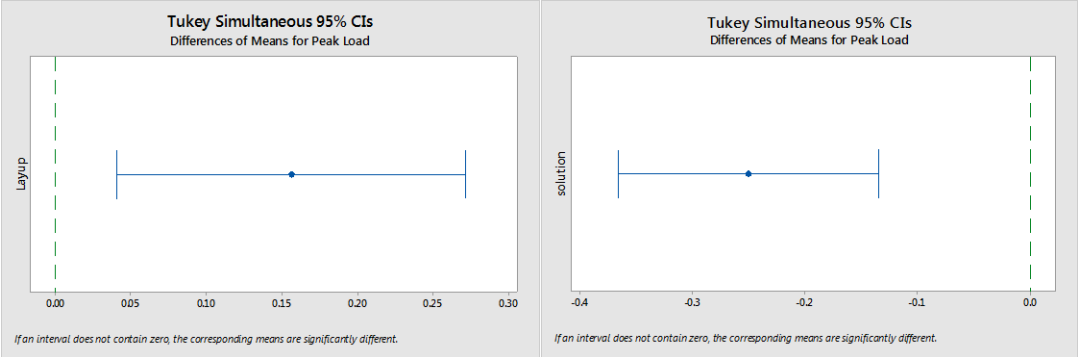

Fig. 49: Tukey's Test Results for Factors Layup and Solution in Step (3)

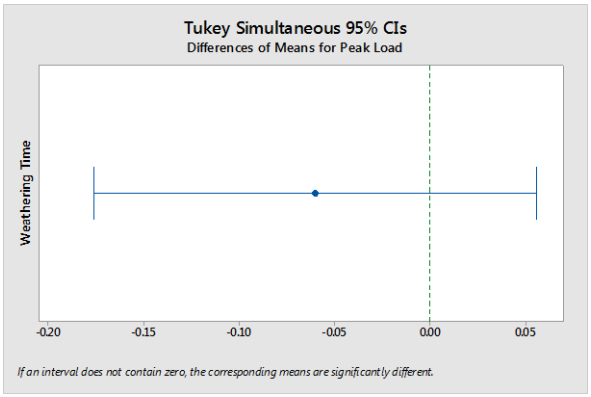

Fig. 50: Tukey's Test Results for Weathering Time in Step (3)

6.3.4 Sample Size Verification

In retrospect to the determination of the necessary sample size, the actual chosen sample size of 7 specimens will be verified according to the gathered experimental results for the blocking factor levels layup 1 and layup 2.

The power analysis will be performed for the factor weathering time because of its amount of levels. There are three levels to be considered. Assuming a significance level of $\alpha = 0.05$, a power of 70.9% for layup 1 and 96.3% for layup 2 was achieved (Fig. 51 and Fig. 52). While the power for layup 2 exceeds the predictions, layup 1 still holds a solid value by which the validity of the results is given. Future studies should be

performed with at least 9 specimens in order to achieve a power of 90% or more, given the same standard deviation.

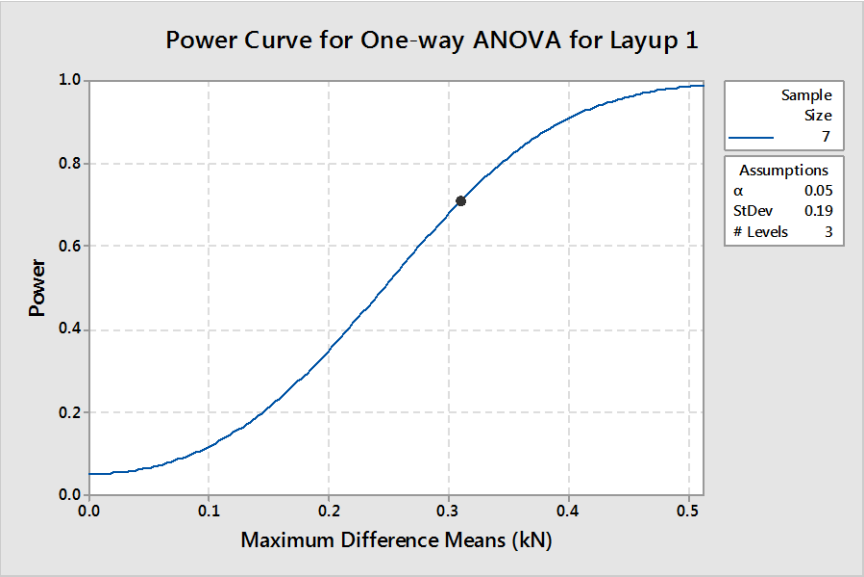

Fig. 51: Verification of Sample Size for Layup 1

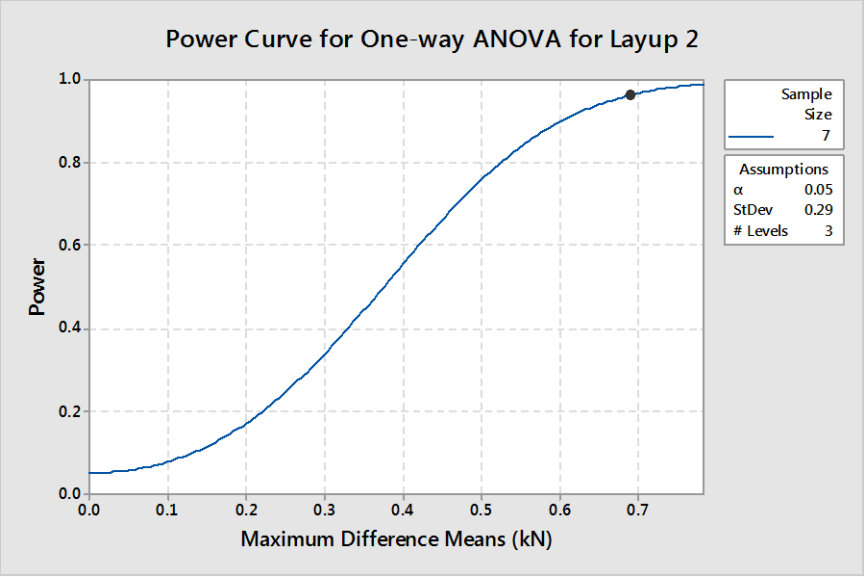

Fig. 52: Verification of Sample Size for Layup 2

6.3.5 Summary

In the following a short summary of the statistical analysis from step (1) through step (3) will be provided. An overview of the response is illustrated in Fig. 53. Therein, the range of peak loads for the drop-weight series is shown. The highest load was borne by layup 2 (L2) with 3.12kN. The lowest values are given with 2.42kN and 2.43kN for layup 1 and layup 2 after 30 days of weathering, respectively. Comparing both layups, the angle ply laminate L2 significantly bore a higher amount of out-of-plane load for both cases, the non-weathered and weathered specimens in the lower salt concentration solution 1 than the cross ply laminate L1. However, exceeding certain salinity, which was reached through a salt concentration of 3.7% (solution 2), the peak loads through impact testing became alike for both layups.

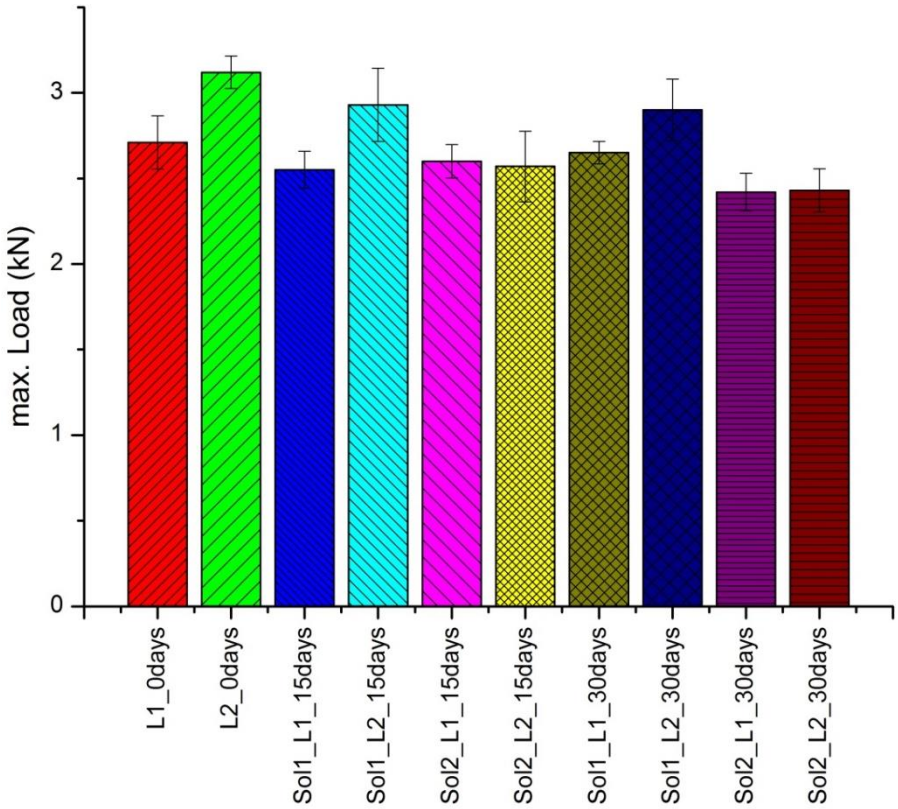

Fig. 53: Comparison of Average Peak Loads for all Weathering Times, Layup and Solutions

Within the first two steps of statistic evaluation, step (1) and step (2), it was found that the weathering time has a significant influence on the response comparing non-weathered and weathered specimens for each solution's concentration individually.

Comparing the different weathering stages exclusively (15 days and 30 days) for both salt concentrations in step (3), no significant difference in the response could be found. Both weathering stages in the accelerated weathering experiment bring about saturated specimens after less than two days as shown in section 6.1 Results Diffusion Study. For this reason, it is concluded that once the material's saturation is reached, no significant change of resistance to out-of-plane impacts can be seen. Regardless of this finding, it has been explained earlier in 2.1.2 Moisture Diffusion in Polymers and Polymeric Composite Materials that a delayed failure mode due to swelling and relaxation is likely to be experienced after prolonged exposure to the accelerated weathering conditions or in case of combined effects of temperature, stress (or strain), and pre-existent damage.

Finally, the sample size of seven specimens for the used experimental design was verified. Nonetheless, a sample size of at least nine specimens would help to increase the power of statements beyond 90%, given the same standard deviations.

7 CONCLUSIONS

In this study, moisture-induced degradation of carbon fiber epoxy composites specimens of varying reinforcement architectures was examined through designed experiments with the assistance of Analysis of Variance (ANOVA).

The completion of this study has resulted in the following pertinent conclusions:

- Successful manufacturing of composite material plates of layups: cross ply laminate $[0°|90°]_{2s}$ and angle ply laminate $[\pm 45°]_{2s}$.
- Using an accelerated weathering method, mass saturation through diffusion at 65°C was reached after 38 hours after immersion of desiccated specimens.
- Diffusion curves and diffusion coefficients of both layups $[0°|90°]_{2s}$ and $[\pm 45°]_{2s}$ did not differ significantly. Both laminated composites possessed the same fiber volume fraction f=55%.
- Peak loads through drop-weight testing were significantly decreased by means of the weathering treatment. Compared to non-weathered specimens, exposure to salt solution at 65°C degraded material after 15 days already. No significant worsening after 30 days could be determined with assistance of ANOVA. Once the composite material was saturated, no significant change of properties occured for the 30 days period at the accelerated diffusion rate.

- It can be concluded that the degradation is more adverse concerning mechanical properties in solutions with higher salt concentrations.
- Comparing both layups, the angle ply laminate significantly bore a higher amount of out-of-plane load for both cases than the cross ply laminate, the non-weathered and weathered specimens in the lower salt concentration. Exceeding certain salinity, in this study reached through the higher salt concentration of 3.7%, the peak loads through impact testing became alike for both layups.

8 REFERENCES

[1] Y. J. Weitsman, *Fluid Effects in Polymers and Polymeric Composites*. Boston, MA : Springer Science+Business Media, LLC, 2012.

[2] P. Mouri, S. Abadi, M. Jeliazkov, T. A. Sebaey, C. S. Lopes, M. Abdalla, and D. Peeters, "Damage Resistance of Dispersed-Ply Laminates," in *20th International Conference on Composite Materials*, 2015.

[3] H. Schürmann, *Konstruieren mit Faser-Kunststoff-Verbunden*, 2nd ed., vol. 2. Berlin: Springer, 2007.

[4] M. Hebert, C.-E. Rousseau, and A. Shukla, "Shock Loading and Drop Weight Impact Response of Glass Reinforced Polymer Composites," *Compos. Struct.*, vol. 84, no. 3, pp. 199–208, 2008.

[5] F. Sarasini, J. Tirillò, L. Ferrante, M. Valente, T. Valente, L. Lampani, P. Gaudenzi, S. Cioffi, S. Iannace, and L. Sorrentino, "Drop-weight impact behaviour of woven hybrid basalt–carbon/epoxy composites," *Compos. Part B Eng.*, vol. 59, pp. 204–220, Mar. 2014.

[6] N. K. Naik, M. N. Joglekar, H. Arya, S. V. Borade, and K. N. Ramakrishna, "Impact and compression after impact characteristics of plain weave fabric composites: effect of plate thickness," *Adv. Compos. Mater.*, vol. 12, no. 4, pp. 261–280, 2004.

[7] Z. Aslan, R. Karakuzu, and O. Sayman, "Dynamic Characteristics of Laminated Woven E-Glass-Epoxy Composite Plates Subjected to Lowvelocity Heavy Mass Impact," *J. Compos. Mater.*, vol. 36, no. 21, pp. 2421–2442, 2002.

[8] E. Zaretsky, G. deBotton, and M. Perl, “The response of a glass fibers reinforced epoxy composite to an impact loading,” *Int. J. Solids Struct.*, vol. 41, no. 2, pp. 569–584, 2004.

[9] Y. Miyano and M. Nakada, “Accelerated testing for long-term durability of various FRP laminates for marine use,” in *Major Accomplishments in Composite Materials and Sandwich Structures: An Anthology of ONR Sponsored Research*, 2009, pp. 3–25.

[10] V. Muliana, A., La Saponara, “Towards an Understanding of the Mechanics underlying Life Performance of Sandwich Construction under Extreme Environments,” in *Solid Mechanics Program – Marine Composites and Sandwich Structures*, 2015, pp. 223–234.

[11] K. V. Pochiraju, G. A. Schoeppner, and G. P. Tandon, Eds., *Long-Term Durability of Polymeric Matrix Composites*, 1st ed. Springer Science+Business Media, LLC, Springer US, 2012.

[12] L. A. Carlsson, “Transport of Sea Water and its Influence on the Tensile Strength of Fiber/Matrix Interface,” in *Solid Mechanics Program – Marine Composites and Sandwich Structures*, 2015, pp. 165–174.

[13] A. Zafar, F. Bertocco, J. Schjødt-Thomsen, and J. C. Rauhe, “Investigation of the long term effects of moisture on carbon fibre and epoxy matrix composites,” *Compos. Sci. Technol.*, vol. 72, no. 6, pp. 656–666, 2012.

[14] P. Davies and Y. D. S. Rajapakse, *Durability of composites in a marine environment*, 1st ed., vol. 208. Springer Science+Business Media Dordrecht, Springer Netherlands, 2014.

[15] J. Crank, *The Mathematics of Diffusion*, 2nd ed. Oxford University Press UK, 1975.

[16] Y. Joliff, L. Belec, M. B. Heman, and J. F. Chailan, "Water Diffusion in Composite Materials – Interfacial Phenomena : Experimental , Analytical and Numerical Approach," in *ECCM15 - 15th European Conference on Composite Materials*, 2012, pp. 24–28.

[17] Y. J. Weitsman and Y. J. Guo, "A correlation between fluid-induced damage and anomalous fluid sorption in polymeric composites," *Compos. Sci. Technol.*, vol. 62, no. 6, pp. 889–908, 2002.

[18] C. L. Soles, F. T. Chang, B. a. Bolan, H. a. Hristov, D. W. Gidley, and A. F. Yee, "Contributions of the nanovoid structure to the moisture absorption properties of epoxy resins," *J. Polym. Sci. Part B Polym. Phys.*, vol. 36, no. 17, pp. 3035–3048, 1998.

[19] Q. ZHENG and R. J. J. Morgan, "Synergistic Thermal-Moisture Damage Mechanisms of Epoxies and their Carbon-Fiber Composites," *J. Compos. Mater.*, vol. 27, no. 15, pp. 1465–1478, 1993.

[20] M. H. Shirangi and B. Michel, "Mechanism of Moisture Diffusion, Hygroscopic Swelling, and Adhesion Degradation in Epoxy Molding Compounds," in *41st Annual International Symposium on Microelectronics, IMAPS*, 2008, pp. 1082–1089.

[21] E. D. Dermitzaki, J. Bauer, B. Wunderle, and B. Michel, “Diffusion of Water in Amorphous Polymers at Different Temperatures Using Molecular Dynamics Simulation,” in *1st Electronic Systemintegration Technology Conference*, 2006, vol. 2, pp. 762–772.

[22] R. Armstrong, S. Slade, and F. Eperjesi, “An Introduction to Analysis of Variance (ANOVA) with Special Reference to Data from Clinical Experiments in Optometry,” *Ophthalmic Physiol. Opt.*, vol. 20, no. 3, pp. 235–241, 2000.

[23] D. C. Montgomery, *Design and Analysis of Experiments*, 8th ed., vol. 2. John Wiley & Sons, 2012.

[24] ASTM D792, “Standard Test Methods for Density and Specific Gravity (Relative Density) of Plastics by Displacement,” vol. 8, no. Reapproved, 2013.

[25] Hexion Inc., “Momentive EPIKOTE Resin MGS RIMR 135 and EPIKURE Curing Agent MGS RIMH 134 – RIMH 137, Technical Data Sheet.” Hexion Inc., pp. 1–8, 2006.

[26] “Salinities in Oceans,” 2016. [Online]. Available: http://www.wasser-wissen.de/abwasserlexikon/m/meerwasser.htm. [Accessed: 01-Mar-2016].

[27] ATSM D1141, “Standard for the Preparation of Substitute Ocean Water,” vol. 98, no. Reapproved, pp. 98–100, 1999.

[28] ASTM D7136 / D7136M, “Standard Test Method for Measuring the Damage Resistance of a Fiber-Reinforced Polymer Matrix Composite to a Drop-Weight Impact Event,” vol. 3, no. Reapproved, 2015.

9 BIBLIOGRAPHY

Armstrong, RA, SV Slade, and F Eperjesi. “An Introduction to Analysis of Variance (ANOVA) with Special Reference to Data from Clinical Experiments in Optometry.” Ophthalmic and Physiological Optics 20.3 (2000): 235–241.

Aslan, Z., R. Karakuzu, and O. Sayman. “Dynamic Characteristics of Laminated Woven E-Glass-Epoxy Composite Plates Subjected to Lowvelocity Heavy Mass Impact.” Journal of Composite Materials 36.21 (2002): 2421–2442.

ASTM D7136 / D7136M. “Standard Test Method for Measuring the Damage Resistance of a Fiber-Reinforced Polymer Matrix Composite to a Drop-Weight Impact Event.” 3.Reapproved (2015)

ASTM D792. “Standard Test Methods for Density and Specific Gravity (Relative Density) of Plastics by Displacement.” 8.Reapproved (2013)

ATSM D1141. “Standard for the Preparation of Substitute Ocean Water.” 98.Reapproved (1999): 98–100.

Carlsson, L. A. “Transport of Sea Water and Its Influence on the Tensile Strength of Fiber/Matrix Interface.” Solid Mechanics Program – Marine Composites and Sandwich Structures. Office of Naval Research, 2015. 165–174.

Crank, J. The Mathematics of Diffusion. 2nd ed. Oxford University Press UK, 1975.

Davies, Peter, and Yapa D.S. Rajapakse. Durability of Composites in a Marine Environment. 1st ed. Vol. 208. Springer Science+Business Media Dordrecht, Springer Netherlands, 2014.

Dermitzaki, E.D. et al. “Diffusion of Water in Amorphous Polymers at Different Temperatures Using Molecular Dynamics Simulation.” 1st Electronic Systemintegration Technology Conference. Vol. 2. N.p., 2006. 762–772.

Hebert, Michael, Carl-Ernst Rousseau, and Arun Shukla. “Shock Loading and Drop Weight Impact Response of Glass Reinforced Polymer Composites.” Composite Structures 84.3 (2008): 199–208.

Hexion Inc. “Momentive EPIKOTE Resin MGS RIMR 135 and EPIKURE Curing Agent MGS RIMH 134 – RIMH 137, Technical Data Sheet.” 2006: 1–8.

Joliff, Y et al. “Water Diffusion in Composite Materials – Interfacial Phenomena : Experimental , Analytical and Numerical Approach.” ECCM15 - 15th European Conference on Composite Materials. Venice (Italy): N.p., 2012. 24–28.

Miyano, Yasushi, and Masayuki Nakada. “Accelerated Testing for Long-Term Durability of Various FRP Laminates for Marine Use.” Major Accomplishments in Composite Materials and Sandwich Structures: An Anthology of ONR Sponsored Research. N.p., 2009. 3–25.

Montgomery, Douglas C. Design and Analysis of Experiments. 8th ed. Vol. 2. John Wiley & Sons, 2012.

Mouri, Peyman et al. “Damage Resistance of Dispersed-Ply Laminates.” 20th International Conference on Composite Materials. Copenhagen: N.p., 2015.

Muliana, A., La Saponara, V. “Towards an Understanding of the Mechanics Underlying Life Performance of Sandwich Construction under Extreme Environments.” Solid Mechanics Program – Marine Composites and Sandwich Structures. Office of Naval Research, 2015. 223–234.

Naik, N. K. et al. “Impact and Compression after Impact Characteristics of Plain Weave Fabric Composites: Effect of Plate Thickness.” Advanced Composite Materials 12.4 (2004): 261–280.

Pochiraju, Kishore V., Gregory A. Schoeppner, and Gyaneshwar P. Tandon, eds. Long-Term Durability of Polymeric Matrix Composites. 1st ed. Springer Science+Business Media, LLC, Springer US, 2012.

“Salinities in Oceans.” URL http://www.wasser-wissen.de/abwasserlexikon/m/meerwasser.htm, 2016. Web. 1 Mar. 2016.

Sarasini, F. et al. “Drop-Weight Impact Behaviour of Woven Hybrid Basalt–carbon/epoxy Composites.” Composites Part B: Engineering 59 (2014): 204–220.

Schürmann, Helmut. Konstruieren mit Faser-Kunststoff-Verbunden. 2nd ed. Vol. 2. Berlin: Springer, 2007.

Shirangi, M H, and B Michel. “Mechanism of Moisture Diffusion, Hygroscopic Swelling, and Adhesion Degradation in Epoxy Molding Compounds.” 41st Annual International Symposium on Microelectronics, IMAPS. N.p., 2008. 1082–1089.

Soles, Christopher L. et al. “Contributions of the Nanovoid Structure to the Moisture Absorption Properties of Epoxy Resins.” Journal of Polymer Science Part B: Polymer Physics 36.17 (1998): 3035–3048.

Weitsman, Y. J., and Ya Jun Guo. “A Correlation between Fluid-Induced Damage and Anomalous Fluid Sorption in Polymeric Composites.” Composites Science and Technology 62.6 (2002): 889–908.

Weitsman, Y. Jack. Fluid Effects in Polymers and Polymeric Composites. Boston, MA : Springer Science+Business Media, LLC, 2012.

Zafar, A. et al. “Investigation of the Long Term Effects of Moisture on Carbon Fibre and Epoxy Matrix Composites.” Composites Science and Technology 72.6 (2012): 656–666.

Zaretsky, E., G. deBotton, and M. Perl. “The Response of a Glass Fibers Reinforced Epoxy Composite to an Impact Loading.” International Journal of Solids and Structures 41.2 (2004): 569–584.

ZHENG, Q., and R.J. J Morgan. “Synergistic Thermal-Moisture Damage Mechanisms of Epoxies and Their Carbon-Fiber Composites.” JOURNAL OF COMPOSITE MATERIALS 27.15 (1993): 1465–1478.